Draft version July 20, 2010
Preprint typeset using LaTeX style emulateapj v. 11/10/09

THE INVISIBLE MAJORITY? EVOLUTION AND DETECTION OF OUTER PLANETARY SYSTEMS WITHOUT GAS GIANTS

Andrew W. Mann[1], Eric Gaidos[2], B. Scott Gaudi[3]

Draft version July 20, 2010

ABSTRACT

We present 230 realizations of a numerical model of planet formation in systems without gas giants. These represent a scenario in which protoplanets grow in a region of a circumstellar disk where water ice condenses and the surface density of solids is enhanced (the "ice line"), but fail to accrete massive gas envelopes before the gaseous disk is dispersed. Each simulation consists of a small number of gravitationally interacting oligarchs (protoplanets) and a much larger number of small bodies that represent the natal disk of planetesimals. Time zero of each simulation represents the epoch at which the gas has disappeared, and the dynamics are integrated for 5 billion years (Gyr). We investigate systems with varying initial number of oligarchs, oligarch spacing, location of the ice line, total mass in the ice line, and oligarch mean density. Systems become chaotic in ~ 1 Myr but settle into stable configurations in 10-100 Myr. We find: (1) runs consistently produce a 5-9 $M_\oplus$ planet at a semimajor axis of 0.25-0.6 times the position of the ice line, (2) the distribution of planets' orbital eccentricities is distinct from, and skewed toward lower values than the observed distribution of (giant) exoplanet orbits, (3) inner systems of two dominant planets (e.g., Earth and Venus) are not stable or do not form because of the gravitational influence of the innermost icy planet. The planets predicted by our model are unlikely to be detected by current Doppler observations. Microlensing is currently sensitive to the most massive planets found in our simulations, and may have already found several analogs. A scenario where up to 60% of stars host systems such as those we simulate is consistent with all the available data. We predict that, if this scenario holds, the NASA *Kepler* spacecraft will detect about 120 planets by two or more transits over the course of its 3.5 yr mission. Furthermore, we predict detectable transit timing variations exceeding 20 min due to the presence of additional outer planets. Future microlensing surveys will detect ~ 130 analogs over a 5 yr survey, including a handful of multiple-planet systems. Finally, the Space Interferometry Mission (SIM-Lite) should be capable of detecting 96% of the innermost icy planets over the course of a 5 yr mission.

Subject headings: celestial mechanics — planets and satellites: dynamical evolution and stability — planets and satellites: formation — planet-disk interactions — planetary systems

1. INTRODUCTION

The overwhelming majority of more than 400 exoplanets detected thus far are gas giants with masses comparable to Saturn or Jupiter (Cumming et al. 2008). Most methods of planet detection, including the Doppler radial velocity technique which has detected the overwhelming majority of the known exoplanets, are biased toward higher planet mass as well as shorter orbital period (Nelson & Angel 1998; Udry et al. 2003; Cumming 2004). Doppler surveys are seriously incomplete for semimajor axes larger than 5 AU, but an extrapolation of a debiased Doppler sample with a "flat" distribution predicts that only ∼17% of planetary systems contain giant planets within 20 AU (Lineweaver & Grether 2003; Cumming et al. 2008). By analyzing the sample of microlensing planet detections in a survey of high-magnification events, Gould et al. (2010) estimate that $36\% \pm 15\%$ of the host stars (with typical mass of $\sim 0.5\ M_\odot$) host giant planets, with $0.02\ M_J < M < 5\ M_J$ per logarithmic decade in separation and mass. By combining the results of Cumming et al. (2008) for planets with $a < 2$ AU with those of Gould et al. (2010) for 2 AU $\lesssim a \lesssim 20$ AU, we estimate that $37\% \pm 13\%$ of stars host giant planets ($m \gtrsim 0.3\ M_J$). We conclude that the fraction of stars hosting giant planets with $a < 20$ AU is likely to be at least 20% but less than 50%.

Thus a substantial fraction, and probably the majority of stars do not host giant planets within $\lesssim 20$ AU. However, studies of star-forming regions of different ages have shown that all or nearly all solar-mass stars begin their lives with disks (Haisch et al. 2001; Lada et al. 2006; Sicilia-Aguilar et al. 2006; Luhman et al. 2008, 2010; Massi et al. 2010). If the accretion of solids is sufficiently rapid and efficient in these disks, then planetary systems are presumably equally numerous around middle-aged stars and the relative paucity of gas giants demands explication. This conclusion is also supported by the limited statistics of debris disks around solar mass stars (Wyatt 2008; Carpenter et al. 2009).

A simple explanation is that gas giants never form around the majority of stars. The core accretion theory of giant planet formation predicts this outcome if disk gas usually disperses before the growth of a sufficiently massive solid core triggers runaway accretion of the gas. The threshold mass is currently thought to be at least 5 $M_\oplus$ (Hubickyj et al. 2005) but depends sensitively on

[1] Institute for Astronomy, University of Hawai'i, 2680 Woodlawn Dr, Honolulu, HI 96822
[2] Department of Geology & Geophysics, University of Hawai'i, 1680 East-West Road, Honolulu, HI 96822
[3] Department of Astronomy, Ohio State University, 140 W. 18th Ave., Columbus, OH 43120

the gas opacity (Ayliffe & Bate 2009). Canonical models of accretion in a minimum-mass Solar Nebula (MMSN) fail to produce a sufficiently massive core at the orbit of Jupiter (Pollack et al. 1996) in the ∼2-6 Myr timescale on which disks are observed to dissipate (Haisch et al. 2001; Hubickyj et al. 2005; Evans et al. 2009). A common explanation for the formation of Jupiter is to include an "ice line" at 3-5 AU where water condenses and the surface density of solids is substantially elevated, promoting core growth (Stevenson & Lunine 1988; Pollack et al. 1996; Kokubo & Ida 2002; Ida & Lin 2004b). Disks around more massive and/or more metal-rich stars presumably have greater amounts of solids, accelerating core accretion (Laughlin et al. 2004; Currie 2009), consistent with the observed correlation of giant planet frequency with host star mass and metallicity (Gonzalez 1999; Fischer & Valenti 2005; Johnson et al. 2007; Kennedy & Kenyon 2008b). Theoretical studies also predict a correlation between disk surface density and the frequency (and mass) of giant planets and lower mass icy planets (Rafikov 2004; Kenyon & Bromley 2009, 2010).

A second explanation is that giant planet formation may be stymied by the tendency of cores to migrate inwards where there is insufficient gas to form a giant planet (Ida & Lin 2008b). This scenario is predicated on the operation of Type I migration in which torques from the gas disk become important for bodies more massive than Mars. The planet-metallicity correlation is explained if cores in disks with more solids grow more rapidly to the threshold of runaway gas accretion, thereby opening up a gap in the disk and halting Type I (but not Type II) migration. However, the magnitude and even the sign of Type I migration remains very uncertain (Li et al. 2009; Muto & Inutsuka 2009; Yu et al. 2010)

Another possibility is that giant planets are ubiquitous but have migrated or been scattered outward (Crida et al. 2009; Veras et al. 2009; Scharf & Menou 2009) to distances where they are detectable only by microlensing when they behave like isolated lenses (Di Stefano & Scalzo 1999a,b; Gould et al. 2007), or by their infrared emission under exceptional circumstances of youth, mass, and proximity to Earth (Debes & Sigurdsson 2006; Kalas et al. 2008; Marois et al. 2008; Thalmann et al. 2009). Finally, giant planets may migrate inwards to disruption within the Roche zone (Pätzold & Rauer 2002), although there are limits on the ubiquity of such occurrences (Pinsonneault et al. 2001; Quillen 2002).

The first two explanations predict that systems lacking gas giants will contain "failed" cores of Earth to Neptune mass that preferentially formed near the ice line (Ida & Lin 2004a; Thommes et al. 2008; Kennedy & Kenyon 2008b; Mordasini et al. 2009). Unless such objects migrated inward, they would remain invisible to the Doppler technique: the signal from a 10 $M_\oplus$ planet at 5 AU is 0.6 m s^{-1}, well below the stability of radial velocity measurements on decadal baselines (Cumming et al. 2008). However, the gravitational microlensing technique is capable of uncovering such planets and several have already been found. Indeed, Sumi et al. (2010) argue that the slope of the mass (ratio) function for planets beyond the ice line is quite steep, such that Neptune-mass planets are ∼ 7 times more common than Jupiter-mass planets. Combined with the Gould et al. (2010) normalization of the frequency of gas giants in this region, this implies that the majority of stars host Neptune or lower mass planets beyond the snow line.

In this paper we investigate a scenario in which several protoplanets or "oligarchs," but not giant planets, have formed at or beyond the ice line at the time disk gas has disappeared. A major premise of our initial conditions is that Type I migration was not effective in these disks. (Type II migration does not act on planets much less massive than Jupiter). We carry out direct numerical integrations of the orbital and mass evolution of these protoplanets as they accrete additional mass from a residual disk of planetesimals. We integrate the orbits of the (proto)planets over 5 Gyr to ascertain the stability of these systems and their configuration at a plausible epoch at which they might be observed.

Our simulations complement the works of Ida & Lin (2008a); Kennedy & Kenyon (2008a); Mordasini et al. (2009), and Thommes et al. (2008). Ida & Lin (2008a) and Mordasini et al. (2009) use analytical models of the orderly growth of cores in disks during the interval that gas is present. They include migration due to torques exerted by the disk, but neglect subsequent, chaotic gravitational interactions between the cores and the residual disk of solids (Ida & Lin 2008b). Thommes et al. (2008) model the dynamical interactions between protoplanets/cores as well as the gas disk but analytically proscribe accretion from a fixed disk of solids. In cases of low disk mass or rapid gas removal, all three investigations predict formation of Earth- to Neptune-sized bodies. Like Kennedy & Kenyon (2008a), our simulations *begin* at the end of the orderly growth phase when the gas has disappeared, and *assume* that no giant planets have formed, but unlike them, we assume that a massive residual disk of smaller bodies is still present.

Our work also contrasts with investigations of the dynamical evolution and configuration of systems of *giant* planets like those detected by Doppler surveys, e.g., Rasio & Ford (1996), Adams & Laughlin (2003), Chatterjee et al. (2008), Raymond et al. (2009a), and Raymond et al. (2010). We expect that the evolution of systems of solid planets that emerge from the icy part of a disk will differ substantially, primarily because the Safronov number

$$S = \frac{v_{\rm esc}^2}{2v_{\rm orb}^2} \quad (1)$$

will be ≤ 1, whereas $S \gg 1$ in systems of giant planets (excluding "hot" Jupiters). More efficient accretion, less intense scattering, and stronger coupling to the planetesimal disk are expected.

The goal of our simulations is threefold: first, we want to predict the evolution and final configuration of such systems for a range of plausible initial conditions. Second, we wish to determine if and how such planets could be detected by present or future means, i.e., the *Kepler* and Space Interferometry Missions (SIM-Lite) and ground-based microlensing surveys. Lastly, we want to establish how measurements of these objects might be used to infer the initial conditions and histories of these systems, especially important given how poorly planet

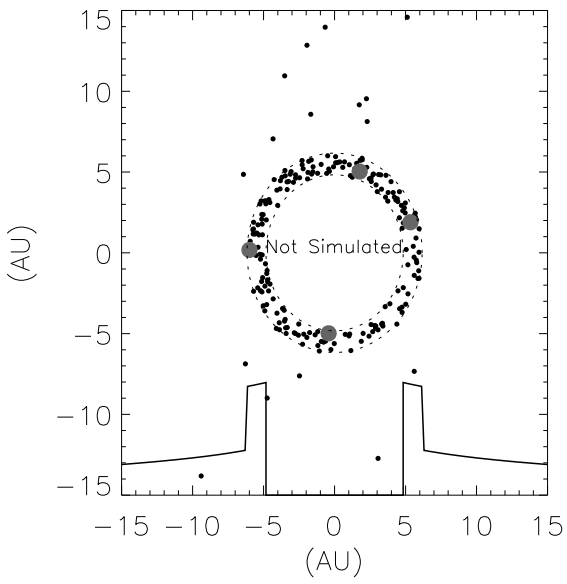

FIG. 1.— Schematic of the typical initial configuration of our systems. Oligarchs are shown in gray in a zone of enhanced surface density between 5 and 6 AU. Small bodies are shown in black and represent a much larger number of planetesimals in the disk. Plotted along the bottom of the graph is an approximation of the logarithm of the surface density of material. Beyond the region of oligarch formation, the density of planetesimals follows a $\Sigma \propto a^{-1}$ mass distribution. The inner system is left empty because this region has only a minor effect on the evolution of the outer system, but requires considerably more time to simulate.

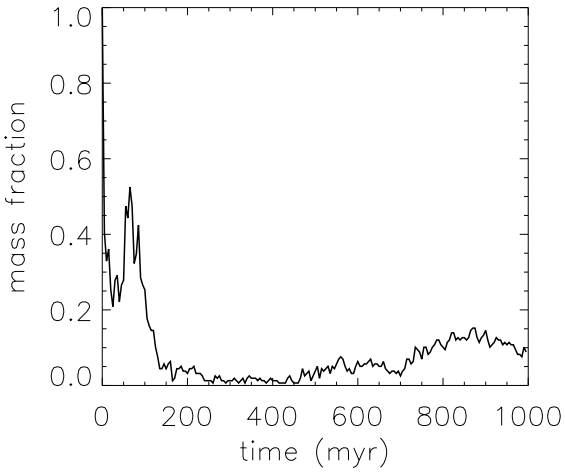

FIG. 2.— Fraction of mass in small bodies within the orbit of the outermost oligarch during the first 1 Gyr for a run from the ST3 set. More than 95% of the mass is in the small bodies at the start of the simulation. By 500 Myr the region has been almost completely cleared of small bodies. Only as the outer oligarch migrates outward do more small bodies enter the region.

formation is understood.

2. METHODS AND MODELS

2.1. *Approach and Assumptions*

Each numerical realization consists of a $1M_\odot$ central star surrounded by a planet-forming disk (Figure 1). Our scenario assumes the canonical theory of planet formation which consists of three phases: (1) runaway accretion of protoplanets from a disk of planetesimals; (2) slower oligarchic growth of these protoplanets as they consume neighboring planetesimals and each other; and (3) a chaotic or giant impact phase when the mass in residual planetesimals falls below that in the protoplanets and the oligarchs' orbits begin to cross (Goldreich et al. 2004; Kenyon & Bromley 2006). The disk includes a region of width $\delta_{\rm ice}$ immediately beyond the ice line ($a_{\rm ice}$) in which the surface density of solids is enhanced by the transport of water vapor out of the inner disk and condensation as ice at $a > a_{\rm ice}$ (Cuzzi & Zahnle 2004; Ciesla & Cuzzi 2006). We assume that oligarchic protoplanets have appeared in this region because of the enhanced density and the relatively short orbital time scale compared to the disk further out. A background disk of unincorporated planetesimals extends from $a_{\rm ice}$ to 400 AU following the surface density profile $\Sigma \propto a^{-1}$ found in observations of protostars (Andrews & Williams 2007). For computational efficiency, we exclude the region outside of 100 AU and the region inside the ice line. A few sets of simulations included inner bodies to assay their effect on the formation of planets further out (Section 2.3).

We assume a disk of solar composition with the total mass within 400 AU of 0.03 $M_\odot$ and a corresponding mass of condensible solids (rock and ice) of ~ 150 $M_\oplus$ (Lodders 2003). The mass of the background disk within the 100 AU simulation region is 43-48 $M_\oplus$, depending on how much mass is moved into the ice line. The additional mass added to the ice line is varied (Section 2.2). We specify the number of oligarchs n and the spacing between them in Hill radii b; this sets the mass of each oligarch and the total mass in oligarchs. The remaining mass, in fact the majority of the mass in all simulations, is distributed evenly among small bodies that represent primordial planetesimals. The number of small bodies is limited by computational resources and is 500 in all of our simulations, except for a single run with 1000. The mass of each small body is about $0.08M_\oplus$, much less than the oligarch masses. We do not model the fragmentation of planetesimals, the production of dust by a collisional cascade, and the removal of that dust by stellar radiation (Wyatt 2008). We discuss the possible consequences of fragmentation on our conclusions in Section 5.3. Oligarchs and small bodies were given non-zero random inclinations ($|i| < 10^{-3}$ and 10^{-2} degrees, respectively) and eccentricities ($e \leq 10^{-3}$ and 10^{-2}, respectively), although we experiment with higher initial i and e values in a single simulation set (see Section 2.3).

The equations of motion of each particle were integrated using the hybrid integrator code Mercury6 with the combination of a second-order, mixed-variable symplectic integrator and the Burlirsch–Stoer integrator for close encounters (Chambers 1999). Mercury6 divides the simulation into large and small bodies. Large bodies interact gravitationally with, and can collide with both large and small bodies. Small bodies also interact gravitationally and collide with large bodies, but they cannot collide with other small bodies. Computations were per-

formed on the TeraGrid network (Catlett et al. 2007). Integrations were performed for 5 Gyr, except for more computationally intensive runs used to check our conditions (Section 2.3). Ten replicate simulations were performed for each set of parameters. The initial positions and orbits were varied slightly between simulations in a set. A timestep of 40 days was used for most simulations, based on the expected orbital period of the innermost oligarch and the requirement that there be at least 10-20 time steps per orbital period, a conservative setting (Raymond et al. 2010). Simulations that included oligarchs in the inner system had a timestep of 8 days, and simulations with a close-in ice line were given a timestep of 20 days. Runs where there were fewer than 10 timesteps per oligarch orbit for an extended period of time were either adjusted, rerun, or had short test simulations run parallel to them to test the accuracy of the results.

For computational efficiency, small bodies in most runs are removed after 1 Gyr. Previous work has shown that this economy will not significantly affect the evolution of the oligarchs if the mass surface density of the small bodies is much less than that of the oligarchs (Kenyon & Bromley 2006). Figure 2 shows the fraction of mass in small bodies inside the orbit of the outermost oligarch for the first Gyr of a run in our standard star. Although at the start of the simulation the small bodies represent the bulk of the mass, by 100 Myr they are less than 50% of the mass in the oligarch region. By 1 Gyr, small bodies account for only $\sim 10\%$ of the total mass. We do not observe significant changes in the orbits of the oligarchs as a result of the removal of the small bodies at 1 Gyr. Oligarchs tend to move into stable orbits long before 1 Gyr. This can be seen in Figures 3 and 4. In a single run from each set we retain the small bodies for 2 Gyr as a check.

2.2. *Parameter Values and Initial Conditions*

Our simulations are described by four principal parameters: $a_{\rm ice}$, $M_{\rm ice}$, b, and n. We also vary the mass density of the oligarchs ρ. Table 1 lists the parameters for our 18 sets, each of which consists of 10 replicate runs. Five additional sets of 10 sensitivity simulations are shown at the bottom of the table and discussed in Section 2.3.

Ice line location: The location of the ice line $a_{\rm ice}$ depends on the opacity and rate of viscous dissipation in the disk and the mass of the central star, and is time dependent (Ciesla & Cuzzi 2006). The ice line in the primordial solar system has been variously placed near 5 AU (to stimulate the rapid formation of Jupiter's core and explain its icy satellites) (Stevenson & Lunine 1988) or at 2.7 AU (to coincide with the transition between hydrated and anhydrous asteroids) (Abe et al. 2000). The position of the ice line presumably varies between planetary disks. In the majority of our simulations, we set $a_{\rm ice} = 5$ AU. In the CI sets (30 runs) $a_{\rm ice}$ was fixed at 2.7 AU.

Ice line mass: Our choice of mass just beyond the ice line is guided by an estimate of the mass of water transported through the inner disk that re-condensed at the ice line, and the mass of solids in the cores of the outer planets in our solar system. To the small amount (< 1 $M_\oplus$) of solids within $a_{\rm ice} < a < a_{\rm ice} + \delta_{\rm ice}$ predicted by a simple $\Sigma \propto a^{-1}$ distribution, we add a fraction of the

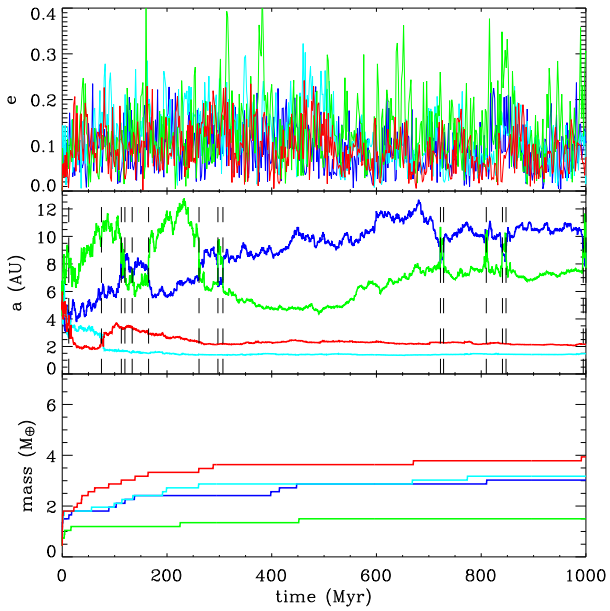

FIG. 3.— Evolution of the system in a run from the ST4 set. Oligarch swaps (exchange of order with distance from the star) are marked with dashed lines, excluding the first 10 Myr when oligarch swaps are more frequent. Because oligarchs often undergo numerous swaps when they approach each other's Hill radius, each dashed line may represent multiple swaps.

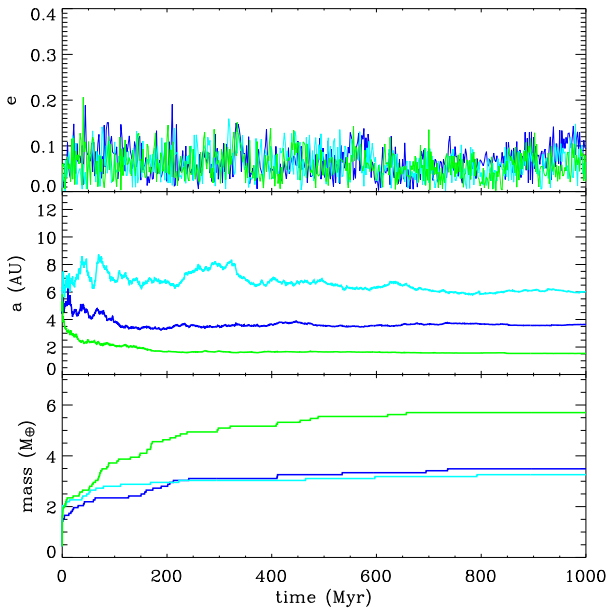

FIG. 4.— Evolution of the system in a run from the ST3 set showing the migration of the innermost migratory planet (IMP) (green). Initially, the IMP (green) migrate inward, while the second and third oligarch (blue and teal respectively) migrate outward through their exchange of angular momentum. All three oligarchs are driven inward at times by their interactions with the planetesimal disk. After ~ 100 Myr the region from 0 to 6 AU has been almost completely cleared of small bodies, causing the inner two oligarchs to settle into relatively stable orbits. This type of angular momentum exchange is common in simulations that start with 3-4 oligarchs.

TABLE 1
Simulation Initial Conditions

Name	b (R_H)	n	$M_{\rm ice}$ ($M_\oplus$)	$a_{\rm ice}$ (AU)	m_i ($M_\oplus$)	'Comments
ST2	8	2	35	5.0	0.44	Standard
ST3	8	3	35	5.0	0.44	Standard
ST4	8	4	35	5.0	0.44	Standard
LM2	8	2	10	5.0	0.44	Low ice line mass
LM3	8	3	10	5.0	0.44	Low ice line mass
LM4	8	4	10	5.0	0.44	Low ice line mass
CI2	8	2	35	2.7	0.44	Close ice line
CI3	8	3	35	2.7	0.44	Close ice line
CI4	8	4	35	2.7	0.44	Close ice line
MP2	5	2	35	5.0	1.78	"Medium packed" oligarchy
MP3	5	3	35	5.0	1.78	"Medium packed" oligarchy
MP4	5	4	35	5.0	1.78	"Medium packed" oligarchy
HP7	2	7	35	5.0	0.70	"Highly packed" oligarchy
HP9	2	9	35	5.0	1.98	"Highly packed" oligarchy
HP12	2	12	35	5.0	3.63	"Highly packed" oligarchy
LD2	8	2	35	5.0	0.44	Low density oligarchs
LD3	8	3	35	5.0	0.44	Low density oligarchs
LD4	8	4	35	5.0	0.44	Low density oligarchs
RD3[a]	~ 8	3	10	5	0.30-0.70	Random m, a of oligarchs
TS3	8	3	35	5	0.44	1000 small bodies
EV3[b]	8	3	35	5	0.44	Earth, Venus included
IO3[c]	8	3	35	5	0.44	Oligarchs in inner system
HE3[d]	8	3	35	5	0.44	Higher initial e, i

[a]The mass of the oligarchs in this system varies randomly by 10% and the semimajor axis by 0.2 AU. b was allowed to vary based on the mass and semimajor axis, but it was not allowed to go below $b = 6$ or above $b = 9$.
[b]This simulation set was run to 100 Myr with a planetesimal disk and then to 1 Gyr without small bodies.
[c]This system has 130 oligarchs in the inner system following a $b = 8$ and $\Sigma \propto a^{-1}$ distribution. The total mass of the inner system was 2.2 $M_\oplus$ spread between 0.5 and 5 AU. This simulation set was run to 100 Myr.
[d]This system has small bodies with $|i| < 10^{-1}$ and $e \leq 5 \times 10^{-2}$ for the small bodies in the region of the oligarchs. This simulation set was run to 250 Myr.

total amount of water from the disk outside this region. We adopt a minimum value of $M_{\rm ice} = 10\ M_\oplus$. Our maximum value ($M_{\rm ice} = 35\ M_\oplus$) assumes all four outer solar system planets formed near the ice line (Thommes et al. 2002) and sums their initial core masses: 10 $M_\oplus$ for Jupiter, 15 $M_\oplus$ for Saturn (Hubbard et al. 2009) and 5 $M_\oplus$ (below the critical threshold) each for Uranus and Neptune. $M_{ice} = 10\ M_\oplus$ and 35 $M_\oplus$ correspond to 15% and 60% of the disk's water in the ice line and a background disk mass within 100 AU of 43 and 48 $M_\oplus$, respectively. Other estimates of the mass in the ice line are similar (Stevenson & Lunine 1988; Kornet et al. 2004; Ida & Lin 2008b).

Oligarch spacing: The spacing between oligarchs is specified as a multiple of the Hill radius,

$$R_H = a \left(\frac{m}{3M_*} \right)^{1/3}, \qquad (2)$$

where m is the initial oligarch mass, and $M_* = 1\ M_\odot$. We use $b = 8$ (Chambers 2006) as well as $b = 5$ (Ford & Chiang 2007; Raymond et al. 2009b, 2010). Additional runs contain "overpacked" oligarchies with $b = 2$ (the approximate Roche limit). This last value is well within the instability limit $b = 3^{4/3}$ where accretion can be rapid (Gladman 1993) but outside horseshoe (1:1 resonance) orbits (Collins & Sari 2009).

Numbers and masses of oligarchs: We vary the number of oligarchs n between two and four in the $b = 5$ and $b = 8$ simulation sets, in analogy to the number of cores that formed at the ice line in our solar system. For the case of $n = 3$ and $a_{\rm ice} = 5$ AU, we fixed the width of the ice line $\delta_{\rm ice}$ to 1 AU (Stevenson & Lunine 1988; Kornet et al. 2004). The initial mass of each oligarch is related to n, $a_{\rm ice}$, and $\delta_{\rm ice}$ by

$$m \approx 3M_* \left(\frac{\delta_{ice}}{nba} \right)^3. \qquad (3)$$

This gives initial oligarch masses of 0.44 and 1.78 $M_\oplus$ for $b = 8$ and $b = 5$, respectively. We subsequently scale $\delta_{\rm ice}$ with $a_{\rm ice}$ and n so that for a given value of b, the initial oligarch mass is unchanged. In the overpacked ($b = 2$) scenario, the requirement that the core mass not exceed 10 $M_\oplus$ (and seed giant planet formation) requires $n > 4$. In these case, we fix the total mass in oligarchs nm as 0.25, 0.50, and 0.75 times the total ice line mass. We calculate n using Equation (3). This gives $n = 12$, 9 and 7 and oligarch masses of 0.7, 1.98, and 3.63 $M_\oplus$, respectively. In any given run, all initial oligarch masses are the same, except for the RD3 simulation set, in which the oligarch mass is allowed to vary slightly.

Oligarch mass density: We use mean densities ρ predicted by Grasset et al. (2009) for planets of 60% ice (15% for the LM sets) and the rest rock. However, super-Earth-mass bodies may retain significant envelopes of H/He gas, giving them mean densities more akin to that of Neptune ($\rho = 1.64$ g cm^{-3}), and this would increase the cross-section for accretion. To investigate this effect, the LD simulation sets were run with $\rho = 1$ g cm^{-3}.

2.3. *Sensitivity Runs*

Larger number of small bodies: The 500 small bodies in each simulation represent a much larger population of planetesimals in the disk. One run (the TP3 set) includes 1000 small bodies, each with half the mass of those in the 500-small body runs. Neither 500 nor 1000 small bodies is physical (there may actually be trillions of planetesimals). The goal here is to ascertain if the results depended sensitively on the number of small bodies or their mass.

Retaining small bodies for 2 Gyr: For a randomly selected run in each set (excluding the CI and HP sets), the small bodies are kept in the simulation for 2 Gyr instead of 1 Gyr. This is done to verify that removal of the small bodies does not create a bias in the results.

Non-identical oligarch masses: A real system of protoplanets will not have identically spaced, identical mass oligarchs. In one set of sensitivity runs (RD3 set) we vary the mass by $\sim$10% and the semimajor axis by $\pm$0.2 AU. In these simulations b is allowed to vary between 7 and 9 as a result of the randomized semimajor axis.

Mass in the inner system: Two sets of runs investigate the effect of mass in the inner system ($a < a_{\rm ice}$) on planet formation in the outer system. In one set (IO3), we include a disk of 130 small (0.002-0.1 $M_\oplus$) oligarchs with a mass surface density $\Sigma \sim a^{-1}$, separation of $b = 8$, and a total mass of 2.2 $M_\oplus$ (the total mass of the inner planets in the solar system). Given that a common outcome of higher-resolution N-body simulations of terrestrial planet accretion are two planets of roughly equal

mass (Raymond et al. 2009c), a second set of runs was performed that included two planets with the masses and orbits of Earth and Venus.

Small Body Eccentricities: Our small bodies start with non-zero but very small values of orbital eccentricity and inclination. However, gravitational perturbations by the oligarchs will drive these values to finite values (~ 0.05) even in the presence of disk gas (Chambers 2006). We run a single set of simulations to 250 Myr with $|i| < 10^{-1}$ and $e \leq 5 \times 10^{-2}$ for the small bodies in the region of the oligarchs.

3. RESULTS

3.1. *Dynamical Evolution*

We are primarily interested in describing the gross dynamical evolution of these systems over the first 1 Gyr, especially when small bodies remain in the system and are being scattered or accreted by the oligarchs. At later times, most (but not all) of the systems do not substantially evolve. We analyze orbital parameters with a resolution of 100 kyr: important events happen on shorter timescales than this, especially in the first 1 Myr of the simulations when systems are most chaotic. However, analysis of such events is not the focus of this work.

TABLE 2
Evolution Statistics

Name	τ_{clear}[a] (Myr)	Resonance Crossings	Frac Order Preserved	Inner Planet Migration (AU)
ST2	290	100	0.6	3.7
ST3	80	470	0.2	3.8
ST4	90	980	0.2	3.7
LM2	450	260	0.7	3.2
LM3	290	820	0.1	3.0
LM4	240	1490	0.1	3.2
CI2	62	50	0.4	2.0
CI3	65	320	0.2	1.9
CI4	56	390	0.3	2.0
MP2	80	70	0.7	3.8
MP3	43	500	0.6	3.8
MP4	36	1297	0.2	3.8
HP7	16	3900	0.1	3.1
HP9	26	11600	0.0	3.3
HP12	66	28600	0.0	3.5
LD2	150	80	0.6	3.8
LD3	74	600	0.3	3.9
LD4	77	1050	0.3	3.8

[a] τ_{clear} is the average time for the disk to lose 70% of it's mass within 10 AU.

We use five metrics to describe the evolution of each system (Table 2): (1) the time τ_{clear} in which 70% of small bodies are removed from inside 10 AU; (2) the number of mean motion resonance (MMR) crossings experienced by the oligarchs with other oligarchs over the first 1 Gyr; (3) the fraction of runs in which two or more oligarchs "swap", i.e., exchange order with distance from the star; (4) the distance of inward migration by the (ultimately) innermost protoplanet; and (5) the number of oligarchs ejected from a system.

Disk clearing: $\tau_{\rm clear}$ is the time over which 70% of small bodies within 10 AU are accreted or ejected. The timescale is not sensitive to the precise choice of outer boundary. $\tau_{\rm clear}$ can be as long as several hundred Myr

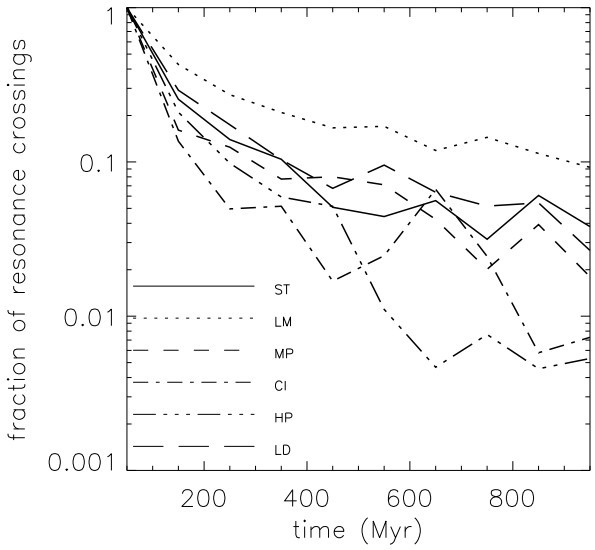

Fig. 5.— Number of MMR crossings in 100 Myr bins, normalized by the first bin. This is a measure of the relative levels of chaos in the system. For our purposes, a resonance crossing occurs whenever an oligarch crosses a 1:1, 2:1, 3:2, 3:1, 4:1, 5:3, or 5:2 mean motion commensurability with another oligarch. Total number of resonance crossings are reported in Table 2.

(Table 2). $\tau_{\rm clear}$ is shorter in systems with more oligarchs (more accreting bodies), lower values of b (oligarchs scatter each other onto more eccentric orbits); a closer ice line (shorter orbital period and dynamical time scale), and lower oligarch mass density (greater cross section of accretion). The LM sets have longer $\tau_{\rm clear}$ values because there is less concentration of mass in the ice line, proximal to the oligarchs. The oligarchs do not grow as quickly nor scatter as efficiently.

Mean motion resonance crossing: We count the number of times an oligarch passes through a 1:1, 2:1, 3:2, 3:1, 4:1, 5:3, or 5:2 mean-motion commensurability with another oligarch (Table 2). The greatest number of MMR crossings occurs in runs with lower values of b and larger n. Figure 5 shows the normalized rate of MMR crossings per time for the six primary simulation groups, binned in 100 Myr intervals. In all cases the rate decreases with time and by 1-3 orders of magnitude over the first 1 Gyr as the systems evolve.

Oligarch swapping: In 43% of the runs in the ST sets, at least one swap (where two oligarchs exchange rank in semimajor axis) occurs between 50 Myr and 1 Gyr. Swapping occurs when two oligarchs approach within two Hill radii (the zone of strong scattering). The oligarchs can collide, or they can enter horseshoe orbits (within a single Hill radius) (Collins & Sari 2009). In the latter case, they often exchange places quickly, usually in $\ll 1$ Myr. Figure 3 shows an extreme case where there are at least 13 distinct swaps over the first 1 Gyr, excluding the chaotic period in the first 50 Myr.

Inner Planet Migration: In all of our primary runs, an oligarch migrates inward to a position between 1 and 3 AU, most often settling between 1.2 and 1.9 AU, i.e. 3-4 AU from its initial starting place. In 81% of cases this body has grown to become the most massive planet in the system. Most runs resemble that of Figure 4. Fig-

ure 3 shows an unusual run in which two inner oligarchs migrate inward. The inward migration of one or more oligarchs is a manifestation of the redistribution of angular momentum in a circumstellar disk and its resulting radial dispersal (Pringle 1981). The angular momentum of the inwardly migrating oligarch(s) is lost to scattered small bodies and some of it is transferred to outwardly migrating oligarchs (Figure 4). This process will occur as long as there is a sufficiently massive disk of small bodies, i.e., for tens or hundreds of Myr (Table 2). Analogous events may have unfolded during the early dynamical evolution of the outer Solar System: Jupiter migrated inward while the other giant planets moved outward as a result of angular momentum exchange through a residual disk of planetesimals (Malhotra 1993; Hahn & Malhotra 1999; Gomes et al. 2005). In our simulations, the Safronov number is less than or not much greater than one, and significant accretion of mass occurs during migration.

Ida et al. (2000) formulated the migration rate of a low mass planet moving through a planetesimal disk as

$$\frac{da}{dt} = \frac{a}{P_K}\frac{4\pi\Sigma_p a^2}{M_*}, \qquad (4)$$

where P_K is the Keplerian orbital period and M_* is the mass of the central star. The migration rate is independent of planet mass. Recast in terms of the ice line mass, the migration timescale is

$$\tau_{\rm migrate} \approx P_K \frac{2a}{\Delta}\frac{M_*}{M_{\rm ice}}, \qquad (5)$$

which as short as ~ 1 Myr for the undepleted disk. The observed migration timescale is slower ($\sim$10 Myr) and is probably in part due to the depletion of the disk by the oligarchs themselves, but may also reflect the inability of our simulations with low numbers of particles to correctly resolve the distribution of planetesimals in horseshoe orbits that most strongly interact with the planet.

Oligarch Ejection: Ejection of oligarchs can occur during the final, chaotic phase of planet formation (Lissauer 1987; Stevenson 1999; Debes & Sigurdsson 2007). An oligarch is considered "ejected" in our simulations if it attains $a > 400$ AU. Ejection of an oligarch is frequent (13 of 30 runs) in the $b = 2$ simulations (Figure 6). In most of these cases, an ejection occurs within 1 Myr after two oligarchs appear to enter a resonance. Resonance between two oligarchs increases their orbital eccentricities, and also excites neighboring oligarchs, and this is sometimes suffcient to eject smaller oligarchs from the system. In a single simulation, two oligarchs stayed near resonance for 100 Myr, causing the ejection of 3 other oligarchs.

3.2. *Configuration at 5 Gyr*

Mass: Figure 7 shows the final system configurations produced by 9 sets of 10 replicate runs (standard, MP, and HP sets) after 5 Gyr. Only 4 of the systems contain a single planet; all started with only $n = 2$ oligarchs. Mass segregation (the tendency of higher mass planets to appear closer to the star) occurs under all conditions (Figure 8). Of the 180 primary runs, $\sim$ 94% produce a planet that ultimately resides between 0.25 and 0.6 $a_{\rm ice}$, and in 78% of all $b = 8$ runs, this planet is the most massive one. This effect is least pronounced in the $b = 2$ set. Approximately one-fourth of the total mass in the ice line is incorporated into these planets. In fewer than half of the runs did the initial innermost oligarch become this innermost planet (Figure 7), in agreement with Chatterjee et al. (2008), who found that in systems of equal-mass gas giants, each planet has roughly equal probability of becoming the innermost. Planet mass decreases with semimajor axis between 0.6 to 2.5 $a_{\rm ice}$. Planets ending outside ~ 2.5 $a_{\rm ice}$ have masses close to that of the original oligarch. These bodies were scattered outside the ice line early in the run and have accreted little mass.

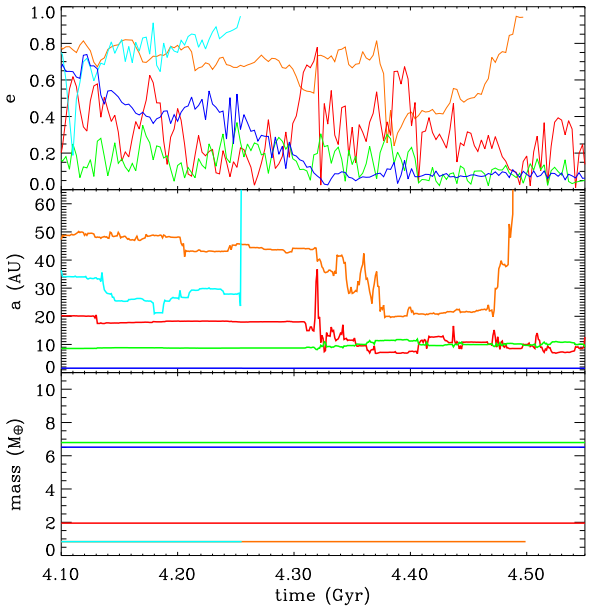

FIG. 6.— Evolution of the system in a run from the HP12 set showing the ejection of two oligarchs (teal and orange bodies) at $\sim$ 4.25 Gyr and $\sim$ 4.5 Gyr.

Eccentricity: We find no correlation between orbital eccentricity and mass, semimajor axis, or number of oligarchs in our runs. Our runs with $b = 2$ (and the most oligarchs) produce a larger dispersion in eccentricity, but this could be a result of the higher total mass in oligarchs. For $b = 8$, no planet ended with $e > 0.3$, and for the ST sets only 2 planets had eccentricities above 0.2. This contrasts with the observed distribution amongst detected planets, and simulations of systems of gas giants (Udry & Santos 2007; Chatterjee et al. 2008; Jurić & Tremaine 2008) (Figure 9). Smaller values of eccentricity are expected in systems where the mass of the oligarchs that perturb each other is lower relative to the mass of the disk of small bodies that dampen such perturbations (Chambers 2006; Raymond et al. 2008).

Dynamical classification: Chambers (2001) describes several dimensionless parameters to compare the outcome of simulations of accretion in the inner solar system to the actual planets. We adopt three, the radial mass concentration RMC, the angular momentum deficit (AMD), and the orbital spacing statistic (OSS), to classify and compare our results. The RMC measures how

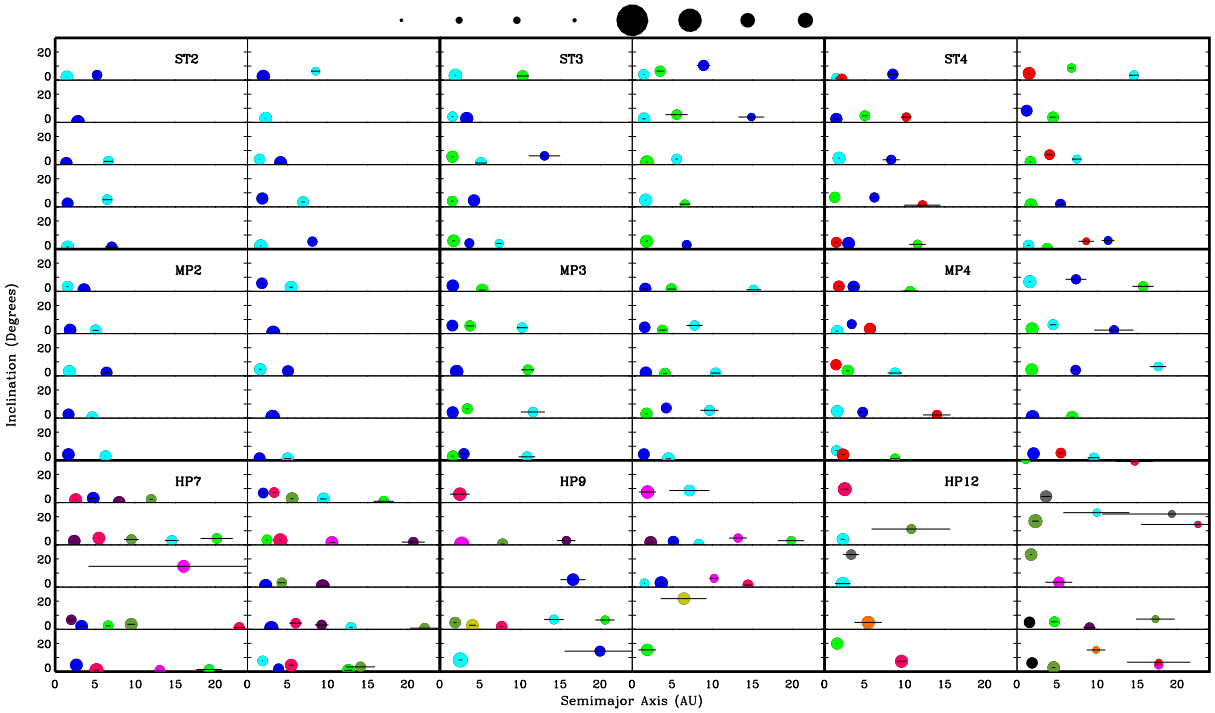

FIG. 7.— Final configuration of all simulations in the ST sets (top), MP sets (middle), and HP sets (bottom). Simulation sets are organized left to right by initial number of oligarchs n, with the fewest on the left. Color coding shows the initial position of the oligarch (blue is initially closest to the star). Each circle represents a planet scaled in size by the planet mass. A line going through the point represents the periapsis and apoapsis of its orbit. As the top is the solar system plotted as a mass (but not distance) scale. Some simulations from the HP sets had planets outside 25 AU, which cannot be seen in these plots.

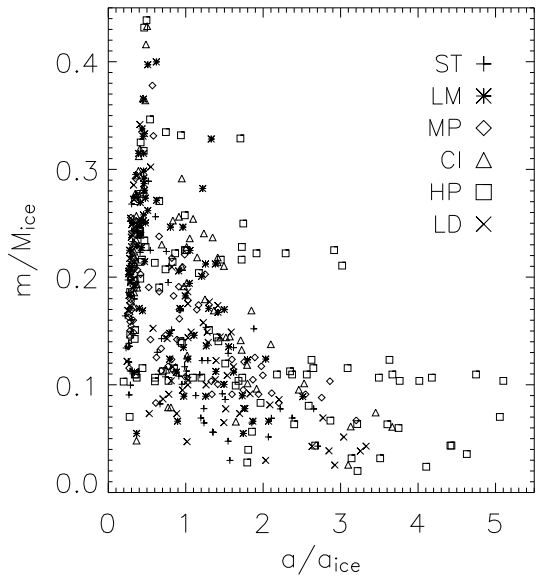

FIG. 8.— Plot of mass vs. semimajor axis scaled by the initial mass and position of the ice line, respectively, for the 6 primary simulation groups. The innermost planets at 0.25 to 0.60 $a_{\rm ice}$ have a clear separation from the other planets. Simulations show a statistical mass segregation effect out to $\sim 2.5\ a_{mboxice}$.

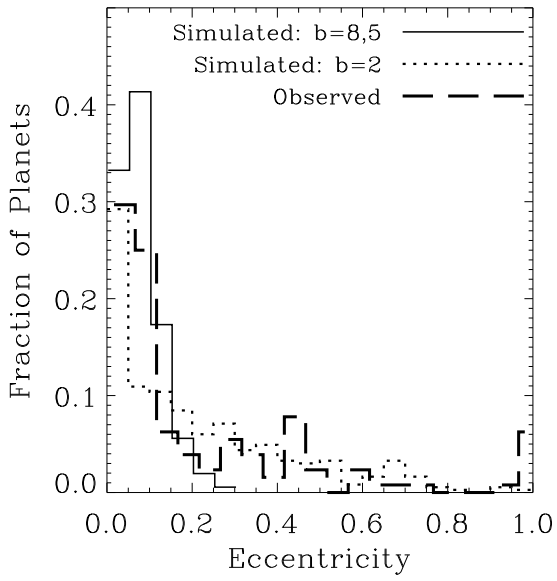

FIG. 9.— Distribution of orbital eccentricities of simulated planets for $b = 8, 5$, and $b = 2$ and known exoplanets (exoplanet.eu). Only a few of our $b = 8, 5$ planets have eccentricities higher than 0.2 whereas the observed gas giant planets span the full range of eccentricities from 0 to nearly 1. The highly packed ($b = 2$) simulations exhibit an eccentricity distribution much closer to observations, which are mostly gas giants.

mass is distributed in the system and is given by

$$\mathrm{RMC} = \max\left(\frac{\Sigma m_j}{\Sigma m_j.[\log_{10}(a/a_j)]^2}\right), \qquad (6)$$

where m_j and a_j are the masses and semimajor axes of the planets in a system. A more tightly concentrated system will have a higher RMC. The AMD is a measure

TABLE 3
Simulation Outcome Classifications

Name	$\overline{M_{tot}}$ ($M_\oplus$)	$\overline{n_f}$	$\overline{OSS}$	σ_{OSS}	$\overline{RMC}$	σ_{RMC}	$\overline{AMD}$	σ_{AMD}
ST2	10.98	1.8	10.32	1.14	13.76	4.75	0.0051	0.0019
ST3	12.76	2.4	8.09	1.81	14.10	5.73	0.0095	0.0070
ST4	12.12	2.8	7.69	1.79	10.79	4.05	0.0093	0.0036
LM2	4.29	1.8	9.60	1.77	21.44	3.87	0.0121	0.0076
LM3	4.93	2.4	8.84	1.39	17.71	5.80	0.0117	0.0058
LM4	5.08	2.8	7.80	1.96	18.32	3.48	0.0152	0.0047
CI2	17.16	2.0	8.17	1.40	15.61	4.97	0.0019	0.0006
CI3	16.99	2.5	7.32	1.48	14.78	3.48	0.0051	0.0021
CI4	16.39	2.4	8.00	1.50	13.03	4.15	0.0050	0.0031
MP2	12.88	1.8	8.41	0.98	16.57	3.64	0.0038	0.0018
MP3	14.22	2.7	7.43	1.60	10.76	3.00	0.0080	0.0037
MP4	15.21	2.9	6.67	0.99	10.68	3.36	0.0076	0.0041
HP7	26.71	4.6	3.85	0.60	9.68	4.00	0.0485	0.1397
HP9	18.67	4.0	5.86	2.19	5.34	4.12	0.1560	0.1747
HP12	14.89	4.2	6.11	2.32	4.74	1.97	0.1413	0.1222
LD2	13.45	1.9	10.12	0.70	11.58	1.58	0.0037	0.0013
LD3	13.17	2.6	8.27	1.83	10.47	2.67	0.0093	0.0049
LD4	13.55	3.0	7.36	1.99	10.34	6.03	0.0093	0.0042
RD3	12.01	2.4	8.66	2.25	14.12	6.01	0.0030	0.0050
TP3	12.05	2.4	7.84	1.73	14.78	5.34	0.0031	0.0018
EV3[a]	11.23	3.7	5.97	0.83	10.28	1.33	0.0167	0.0096
IO3[a]	11.74	30.9	1.11	0.11	8.38	4.00	0.0521	0.0124
HE3[b]	10.55	2.7	7.43	0.75	21.12	6.92	0.0082	0.0038

[a]Configuration at 100 Myr.
[b]Configuration at 200 Myr

of orbital excitation and is given by

$$\mathrm{AMD} = \frac{\Sigma_j m_j \sqrt{a_j}[1 - \sqrt{(1-e_j^2)}\cos i_j]}{\Sigma_j m_j \sqrt{a_j}}, \qquad (7)$$

where i_j and e_j are the inclinations and eccentricities of the planets in a system. The AMD measures the difference between the angular momentum (in the z-direction) of a system and that of a system of identical bodies on circular, non-inclined orbits with the same semimajor axes. The OSS is a measure of the mean spacing of planets and is given by

$$\mathrm{OSS} = \frac{1}{N-1}\left(\frac{a_{\max} - a_{\min}}{a_{\max} + a_{\min}}\right)\left(\frac{3M_*}{2\bar{m}}\right)^{1/4}, \qquad (8)$$

where N is the number of bodies, $a_{\max}$ is the maximum semimajor axis, $a_{\min}$ is the minimum semimajor axis, M_* is the mass of the central star, and $\bar{m}$ is the mean mass of the oligarchs. Unlike the RMC, the OSS ignores the mass and location of individual oligarchs and depends on the distance between the bodies.

These statistics have no meaning for single-planet systems and those cases are excluded from the calculations. Average values and standard deviations of RMC, AMD, and OSS for each set of simulations are listed in Table 3 along with values for a number of exoplanetary systems and the solar system. These data are also plotted in Figure 10. Although there is considerable spread in these statistics between the simulations, with the exception of the HP ($b = 2$) run, they occupy a region not spanned by known planetary systems, most of which contain gas giants. Our predicted systems all have OSS > 6, in contrast to known expoplanet systems, but this is likely an artifact of the detection bias for close-in planets. Our systems have intermediate values of RMC (8-20) that are poorly represented by the current catalog of known multi-planet systems.

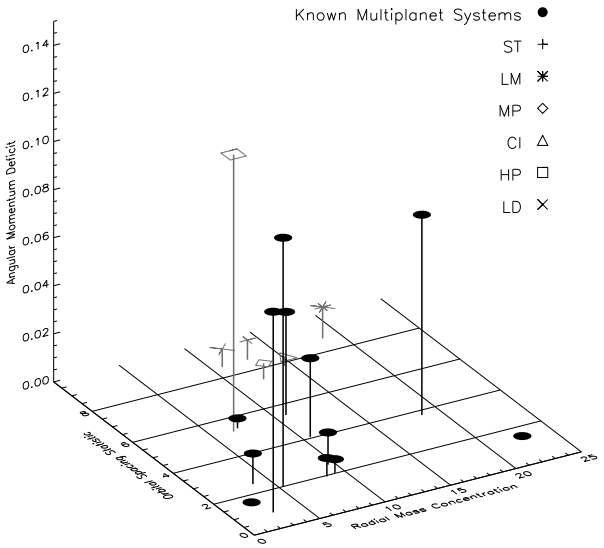

Fig. 10.— Average OSS, RMC, and AMD for the 6 primary simulation groups alongside 12 known planetary systems with ≥ 3 planets as well as the solar system values. Most of the observed exoplanet systems shown contain at least 1 gas giant. Since inclinations are measured from an invariable plane, which is not known or poorly defined for exoplanetary systems, we assume zero inclinations for these calculations. Although the known planets cover a wide range of values, they are clearly very different from our simulations with the exception of the HP ($b = 2$) runs.

Mean motion resonances: Because of migration, two planets may enter an MMR where the orbital periods are integer ratios. The resonant angle ϕ:

$$\phi = pL_1 - qL_2 - m\bar{\omega}_1 - n\Omega_1 - r\bar{\omega_2} - s\Omega_2, \qquad (9)$$

must librate between two values, where p, q, m, n, r, s are integers, L is the mean longitude, $\bar{\omega}$ is the argument of periapsis, and Ω is the longitude of the ascending node. The subscripts 1, 2 refer to the inner and outer planet respectively. Outside MMR, the resonant angle will be unbounded (i.e., will circulate) (Elliot et al. 2005). We searched the final billion years of the 180 primary simulation sets for 1:1, 2:1, 3:2, 3:1, and 4:1 MMRs. We required any MMR to last at least 100 kyr. None of our systems appear to have had a MMR in that interval. Even a system that appears to be in 1:1 commensurability (see far bottom right of Figure 7), did not have a bounded resonant angle.

Inner system: Two sets of runs (Figures 11 and 12) in which mass (planets or oligarchs) was placed inside the ice line show that this has little effect on the dynamical evolution and final configuration of the outer planets. The innermost ice line planets were 0.1-0.2 AU further out at 100 Myr, and in the IO3 set they had accreted an average of 0.3 $M_\oplus$ more mass (from the inner system). Other effects on the outer planets were non-systematic

or negligible. However, the effect of the outer planets on the inner system were significant. Figure 11 shows the configuration of the EV3 system after 100 Myr. In all 10 runs the Earth and Venus analogs collided after 15-70 Myr (and accreted some small bodies), forming a single 2-3 $M_\oplus$ planet at a median semimajor axis of 0.81 AU (Figure 11). In each simulation, this coincides with the time when the innermost of the outer planets migrates inside of 2.5 AU. In companion runs with Earth and Venus analogs but no outer planets, no such collision ever occurs. After the small bodies have been artificially removed, the configurations remain stable for at least 1 Gyr. Figure 12 shows the 100 Myr configuration of systems that started with a disk of inner oligarchs rather than two planets. On average, 1.5 $M_\oplus$ of the initial 2.2 $M_\oplus$ inner disk mass has been scattered outward or accreted by the outer oligarchs. Amongst the 10 runs the largest surviving body in the inner system has a mass of 0.53 $M_\oplus$.

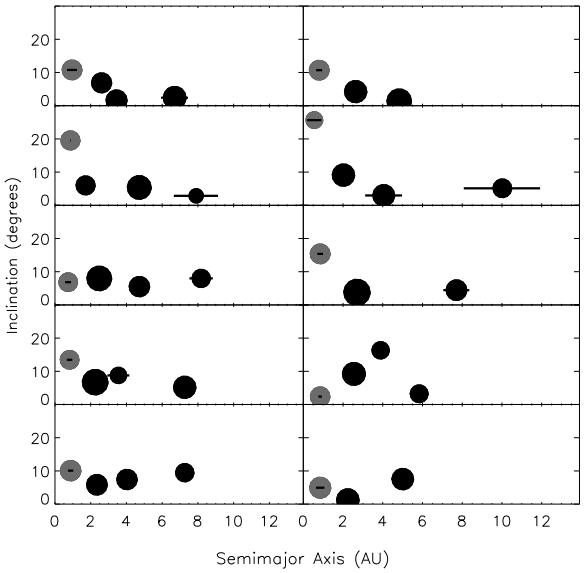

FIG. 11.— Configuration of the EV3 set after 100 Myr. The planet formed from the collision of the Earth and Venus analogs is shown in gray. This collision occurs in all 10 simulations, forming a $2-3$ $M_\oplus$ planet. The innermost planet in the system idoes not migrate in as far inwards as in the runs where no inner mass is included, but otherwise the system is similar to the ST3 set.

Accretion onto the central star: There are two competing explanations for the observed correlation between high metallicity and the presence of giant planets. One is that higher metallicity augments the mass of solids in a planet-forming disk, allowing cores to form gas giants before the gas dissipates. The other is that rocky material has been accreted onto the stellar photosphere during planet formation (Gonzalez 2006). Because systems without detectable gas giants are not statistically more metal-rich than solar, one check of our scenario is the amount of mass that falls onto the central star. An amount sufficient to significantly increase the metallicity of the photosphere would conflict with observations. We assume that a solar mass star had a convective region of 0.02 $M_\odot$ at 1 Gyr, (Asplund et al. 2009; D'Antona & Mazzitelli 1994) and that solids have the composition of carbonaceous chondrites (Fe is 20% by mass) (Grevesse & Anders 1989). In our 180 primary simulations without mass in the inner system, the average mass accreted onto the parent star is 0.9 ± 0.8 $M_\oplus$. For the EV3 and IO3 sets, the average is 0.3 ± 0.1 $M_\oplus$ and 3 ± 1 $M_\oplus$ respectively. The highest value in any run is 4.8 $M_\oplus$, corresponding to ~ 1 $M_\oplus$ of iron. The corresponding increase in [Fe/H] is no more than 0.06 dex and more typically ~ 0.02 dex. The actual metallicity enhancement is likely to be smaller because the convective zone of solar-mass stars is much larger at $t < 30$ Myr when much of the mass is accreted (Ford et al. 1999). Thus our scenario does not conflict with observations.

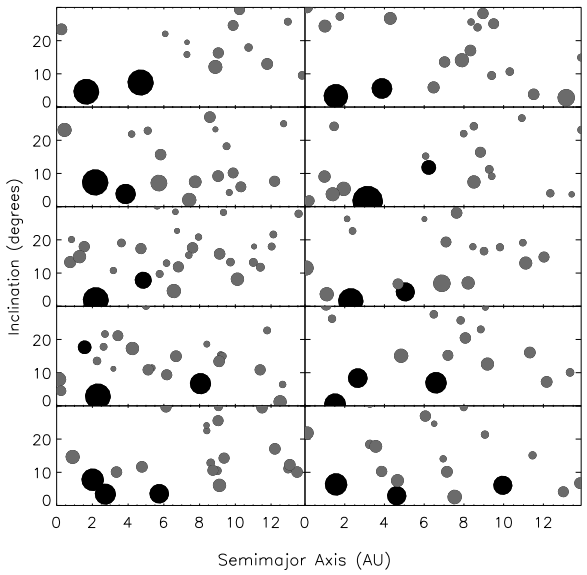

FIG. 12.— Configuration of the set starting with 130 oligarchs in the inner system after 100 Myr. Apoapsis and periapsis lines like those in Figures 7 and 11 are suppressed. The surviving inner system oligarchs are shown in gray. In most cases the inner system oligarchs were thrown onto high inclination orbits outside of the inner system or accreted by an inward migrating oligarch. There is no obvious pattern to the distribution of the (initially) inner system oligarchs.

3.3. *Sensitivity Runs*

The TP3 runs contain twice as many small bodies (1000) than the other runs, but produce systems with the same mean number of planets, and similar values of $\overline{M_{\rm tot}}$, $\overline{\rm OSS}$, $\overline{\rm RMC}$, $\overline{\rm AMD}$ compared to the ST3 set (Table 3). The only major difference was that there was less variation between the 5 Gyr configurations produced by the TP3 runs. The standard deviation of AMD, OSS, and RMC are all lower, presumably because random fluctuations are reduced with a larger number of small bodies. We conclude that in most of our simulations, the between-run variability is exaggerated due to the use of a finite number of small bodies.

Simulations in which the small bodies were removed at 2 Gyr as opposed to 1 Gyr did not result in significantly different systems. Most systems, including both oligarchs

and small bodies, achieve a degree of stability earlier than 1 Gyr. Runs where the initial masses, position, and Hill spacing of the oligarchs vary slightly (Table 1) did not produce significantly different systems.

Simulations run with higher eccentricities and inclinations for small bodies nearby the oligarchs showed slower initial mass growth than the standard set. At 100 Myr, the HE3 set had $\sim 4\ M_\oplus$ less mass in oligarchs than the ST3 set. By 250 Myr, the difference was only $\sim 2\ M_\oplus$. This result supports our expectation that because the Safronov numbers are low, oligarchs ultimately accrete all planetesimals in their zone. Inner planet migration is minimally affected by the higher eccentricities and inclinations. At 100 Myr the innermost planet is, on average, < 0.2 AU further out in the HE3 set than in the ST3 set. At 250 Myr, the difference is negligible.

4. PROSPECTS FOR DETECTION

Our simulations are useful to the extent they can make testable predictions. We investigate the prospect of detecting the 534 planets predicted by our 180 primary simulation sets. We divide the expected detections up by initial conditions to determine which initial conditions were most accurate when detections are made. Figure 13 shows their masses and semimajor axes relative to the detection domains of Doppler radial velocity, ground-based microlensing techniques, the NASA *Kepler* mission, and the proposed SIM-Lite. Until there are substantial improvements in sensitivity and stability (Eggenberger & Udry 2010), Doppler is unlikely to detect any of the predicted planets. The other three techniques will be able to detect at least some of these objects.

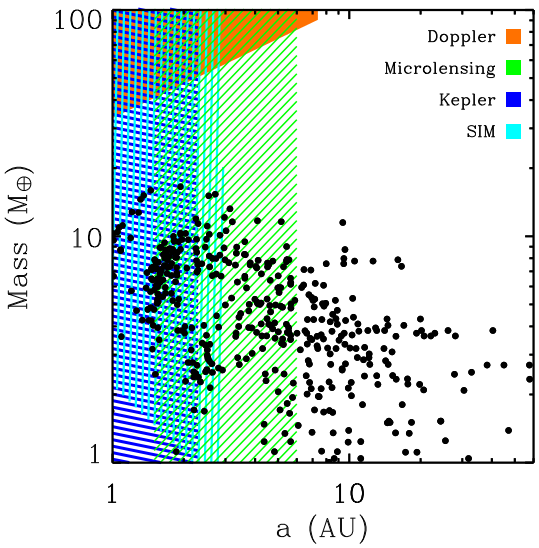

FIG. 13.— Final mass and semimajor axis of all planets from the primary 6 sets and the detection domains of 4 planet-finding techniques. The Doppler range is set by a Doppler amplitude of $K = 3$ m s^{-1}. A *Kepler* detection requires observation of at least 2 (rather than the usual 3) transits, and we assume a mission lifetime of 3.5 years, so planets with period $P > 1.75$ yr will not be detected. Microlensing is most sensitive in the 1.5-6 AU range, where the planet detection probability is at least 1% per microlensing event. The SIM-Lite range is set by a detection probability $> 85\%$ (see Equation (17) in the text). Although SIM might be able to detect planets with P greater than the lifetime of the mission (~ 5 yr) we conservatively exclude such planets.

4.1. *Microlensing*

Microlensing is currently the only ground-based detection method that is sensitive to the planets predicted by our simulations. Microlensing is most sensitive to planets with projected separations near the Einstein radii $R_{\rm E}$ of their primaries, corresponding to $R_{\rm E} \sim 3.5\ {\rm AU}(M_*/M_\odot)^{1/2}$ for typical lens and source distances. Thus for a typical primary mass in current surveys of $\sim 0.5\ M_\odot$ (Gould et al. 2010), the sensitivity of microlensing peaks for planets with semimajor axes ~ 3 AU. Current microlensing surveys can detect planets with mass $\gtrsim 3\ M_\oplus$ with separations within a factor of a few of this distance. Indeed, several of the microlensing planets detected to date have masses in the range $3 - 15\ M_\oplus$ and projected separations of $1 - 3$ AU (Beaulieu et al. 2006; Gould et al. 2006; Bennett et al. 2008), and thus may be analogs to our simulated systems. Interestingly, for the planet OGLE-2005-BLG-169Lb with mass $\sim 13\ M_\oplus$ and projected separation ~ 2.7 AU, Gould et al. (2006) exclude additional Jupiter-mass planets within the range of projected separations of $0.5 - 15$ AU; indicating that this may indeed by a system without gas giants.

We can estimate the expected number of microlensing detections one would expect, assuming that 60% of stars have systems such as those we simulate. Using the standard set, for each system we randomly choose a primary lens mass according to an event rate distribution

$$\frac{d\Gamma}{d\log M} \propto M^{1/2}\frac{dN}{d\log M} \qquad (10)$$

for a mass function $dN/d\log M \propto M^{-\alpha+1}$. We adopt $\alpha = 0.2$ and restrict our primary masses to the range $0.05 - 1\ M_\odot$, with an average primary mass of $\sim 0.5\ M_\odot$. We assume the planets in the system are coplanar and draw a random inclination i for the system distributed as $\cos i$. Then, for each planet, we compute its mass ratio and projected separation, drawing a random orbital phase for each planet, ignoring the (small) effects of non-zero eccentricities. We then scale the projected separation to the Einstein radius, assuming $R_{\rm E} = 3.5\ {\rm AU}(M_*/M_\odot)^{1/2}$. Finally, we determine which of the planets in the system are detected in each of the 13 events in the Gould et al. (2010) sample, noting instances when multiple planets are detected. We repeat this for all of the simulated systems and for 5000 Monte Carlo trials. We find that Gould et al. (2010) should have detected ~ 1.7 planets, with an expected mean mass ratio of $\sim 10^{-4}$, and maximum mass ratio of $\sim 10^{-3.5}$. In fact, Gould et al. (2010) found one system with mass ratio $\sim 10^{-4.1}$ (OGLE-2005-BLG-169Lb), and two systems with mass ratio $10^{-3.5}$, consistent with our scenario.

Figure 14 shows the observed cumulative distributions of mass ratios from the Gould et al. (2010) sample, compared to the expected distributions for a scenario in which 60% of stars host planets with the properties of the standard simulation set, and 30% host four giant planets with the masses and semimajor axes of the solar system. The remaining 10% of giant planet systems host close-in planets currently undetectable by microlensing. The number of expected detections and the distribution

of mass ratios are both broadly consistent with the observed sample of events. We conclude that this scenario is consistent with all available constraints.

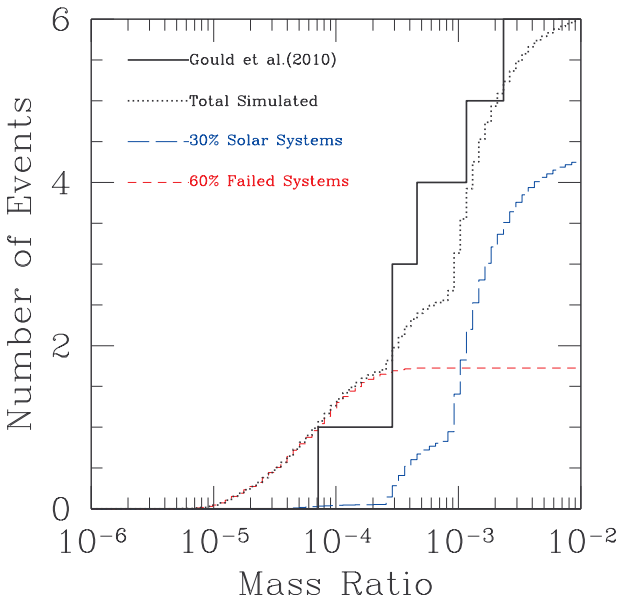

FIG. 14.— The solid line shows the cumulative distribution of mass ratios for the six detected planets in the four year sample of 13 microlensing events monitored by the μFUN collaboration (Gould et al. 2010). The dotted line shows the cumulative distribution of mass ratios predicted for this sample, based on the detection efficiencies of the monitored events, and assuming a model in which 30% of stars have four giant planets with masses and semimajor axes equal to Jupiter, Saturn, Uranus, and Neptune, and 60% of stars have systems of planets predicted by our standard simulation set. These predictions assume a power-law distribution of primary masses, with a mean mass of $\sim 0.5 M_{\odot}$.

What are the prospects for detecting analogs to the systems we have simulated in future microlensing surveys? We consider the two classes of microlensing surveys that are likely to take place over the next 10 years: alert and follow-up monitoring of high-magnification events similar to that already being conducted, and "next-generation" surveys in which thousands of low-magnification events are detected and simultaneously monitored with the ~ 10 minute cadence needed to detect Earth-mass planets using an array of $1-2$m telescopes with wide field-of-view cameras. See (Gaudi et al. 2009) for further discussion of these two channels.

For the high-magnification event channel, we follow the method outlined above to simulate the number of expected detections, except we assume that 20 events per year with maximum magnification > 100 are densely monitored during each peak. This represents a factor of ~ 6 improvement over the rate in Gould et al. (2010), which should be realizable with the expected better prediction of high-magnification events, increased number of alerts, and decrease in the maximum magnification threshold from 200 to 100 (Gould et al. 2010). We adopt the analytic detection sensitivity estimate discussed in (Gould et al. 2010), assuming $\eta = 0.32$ and $\xi = 100$. The results are shown in Table 4, for the six primary simulation sets. We expect an average of 4.6 planet detections per year (for the standard set), with roughly one detection of a multiple-planet system per year. For the HP simulation set, we find that there is a significant chance (0.17 per year) of detecting as many as four planets in the same event, whereas these probabilities are generally substantially smaller ($\leq$0.03 per year) for the other simulations. This indicates it may be possible to distinguish between the various input assumptions of the simulations using observations of multiple planet systems.

For the low-magnification events detected in next-generation surveys, we use the unpublished simulation code of Gaudi, Han, and Gould. This code simulates ensembles of planetary microlensing events and estimates detection rates for a given input value of the mass and semimajor axis of the planet. The simulated light curves account for the effects of weather, variable seeing, moon and sky background, and the finite size of the source star. We assume parameters similar to that expected for the funded Korean Microlensing Telescope Network next-generation microlensing survey: three 1.6m telescopes with 4 deg^2 cameras located in Australia, Chile, and South Africa (C. Han, pers. communication). The host lenses are drawn from a model of the Galactic population of lenses and sources that matches available constraints (Han & Gould 1995, 2003). The resulting detection probability for each of the planets in the 180 simulations is shown in Figure 15, and the expected number of detections per year are listed in Table 4. We predict that next-generation surveys should detect ~ 22 planets in low-magnification events per year (for the standard set), assuming that 60% of all stars host planetary systems such as those we simulate. These detections are

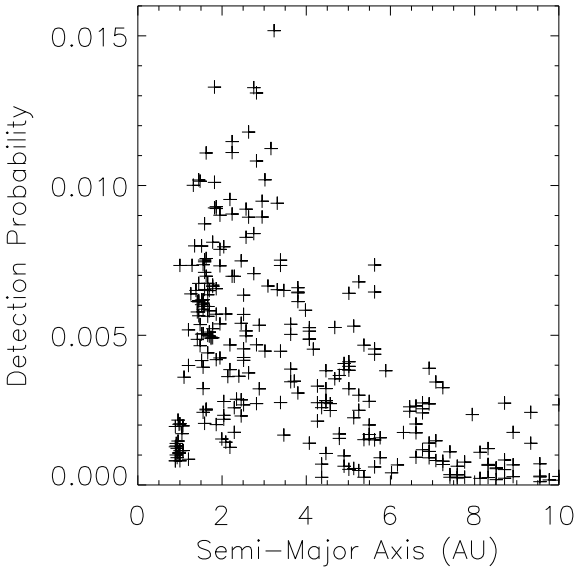

FIG. 15.— Probability of detecting the planets from our 180 primary simulation sets in a next-generation, ground-based microlensing survey, consisting of three 1.6m telescopes with large FOV cameras located in Chile, South Africa, and Australia. The higher detection probabilities near $\sim 2-3$AU are caused by their proximity to the Einstein ring and the tendency for closer in planets to have higher masses (Section 3.2). Assuming 60% of stars systems analogous to those in our primary simulation sets, such a next-generation ground-based microlensing survey would detect ~ 22 planets per year (see Table 4).

TABLE 4
Detection Statistics

Name	Kepler[a]	SIM[b]	Microlensing[c]			TTV[d]	Transit Prob[e]
			(low-mag)	(high-mag)		(min)	(%)
				Total	M-P Sys[f]		
ST	128.9	39.8	22.4	4.63	1.07	34.3	0.30
LM	7.0	34.3	13.2	2.15	0.52	73.2	0.19
CI	344.9	55.3	23.7	5.86	1.66	14.8	0.47
MP	105.7	39.4	24.9	5.58	1.48	32.6	0.29
HP	42.8	32.3	22.8	5.98	1.26	54.2	0.21
LD	119.2	38.6	22.4	4.89	1.13	38.1	0.28
Average	124.8	39.9	21.1	4.62	1.08	41.2	0.28

[a]Here, a Kepler detection counts if ≥ 2 transits are observed over the 3.5 yr Kepler mission. We assume $\sim 60\%$ of stars have systems similar to those in a given simulation set.
[b]Number of detections by SIM-Lite assuming 64 target stars and that $\sim 60\%$ of stars have systems similar to those of a given simulation set.
[c]The number of microlensing detections per year assuming $\sim 60\%$ of stars have systems similar to those of a given simulation set.
[d]Median transit timing variation for the innermost planets in a given simulation set.
[e]Median transit probability for innermost planet in a given simulation set.
[f]Number of systems with more than one planet detected in a single microlensing event.

in addition to those found in high-magnification events. Multiple-planet systems will be rare (detection probabilities of $\lesssim 0.1\%$) in these low-magnification events.

While ground-based surveys are relatively insensitive to the low-mass, large semimajor axis planets we typically find in our simulated systems, a space-based microlensing survey (Bennett & Rhie 2002; Bennett et al. 2009; Beaulieu et al. 2010) would be exquisitely sensitive to these bodies (and essentially all of the planets we find in our simulations). In particular, a space-based microlensing survey would detect the most distant planets with $a \gtrsim 15$ AU as isolated, short time scale events without the signature of the host star (Han et al. 2005).

4.2. *Kepler*

The *Kepler* spacecraft was successfully launched on 2009 March 6 and is continuously monitoring $\sim 10^5$ F- to K-type stars with the primary objective of discovering transiting Earth-mass planets on 1 AU (1 yr period) orbits (Koch et al. 2010), although the detection of many planets on shorter-period orbits is expected, e.g., Selsis et al. (2007). Three transits will be required to confirm a planet; hence the 3.5 yr nominal mission lifetime. However, Yee & Gaudi (2008) point out that *Kepler* should detect one or two transits by planets on more distant orbits. The innermost planets in our 180 primary simulation runs have a median $a = 1.66$ AU ($P = 2.14$ yr), making it possible that two (but usually not three) transits would be observed, geometry permitting. We calculated the expected number of such planets that *Kepler* will detect transiting at least twice using Equations (2) and (4) from Yee & Gaudi (2008), assuming that 60% of all solar-type stars have such systems, and ignoring the effect of eccentricity. (The median eccentricity is 0.08). We use *Kepler's* precision given in Jenkins et al. (2010) and the characteristics of *Kepler's* target stars from Batalha et al. (2010). The predicted number of transit detections is 129 for the standard set, and will be larger if ice lines are located closer to stars (See Table 4). Around a solar mass and radius star *Kepler's* detects a transit with a signal-to-noise ratio (S/N)

$$S/R \approx 10 \left(\frac{R_*}{R_\odot}\right)^{-3/2} \left(\frac{M_*}{M_\odot}\right)^{-1/6} \left(\frac{r_p}{R_\oplus}\right)^2 \left(\frac{P}{3.5\ yrs}\right)^{1/6} 10^{-0.2(V-12)}, \quad (11)$$

where R_* and M_* are the radius and mass of the star, r_p is the radius of the planet, and P is the period of the planet (Yee & Gaudi 2008). The radius of a 10 $M_\oplus$ body composed of equal parts water ice and rock/metal is predicted to be 2.3 $R_\oplus$ (Grasset et al. 2009). At the median semimajor axis of our innermost planets ($a = 1.66$ AU, $P = 2.14$ yr) a planet orbiting a $V = 12$, Sun-like star would produce a transit with a depth of 0.4 mmag and a S/N of ~ 50. The depth and S/N will be larger if the planet has a thick atmosphere.

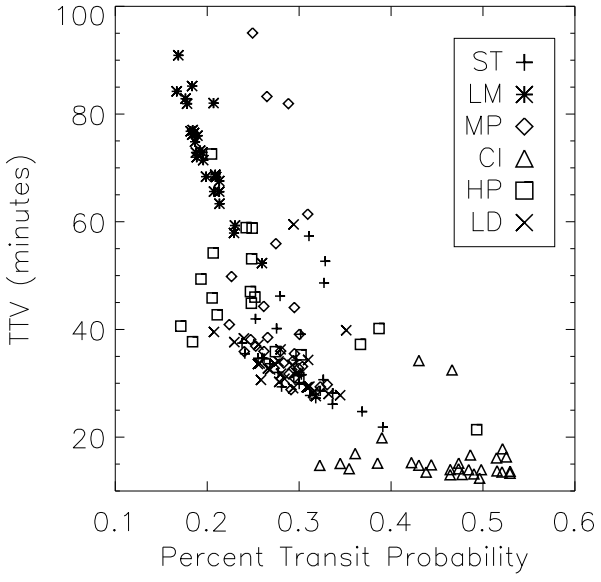

Fig. 16.— Transit timing variations vs. transit probability of the innermost planets predicted by our simulations. The TTV is the absolute difference in the time of transit center between successive transits, averaged over successive transits. The estimated TTV precision of *Kepler* (1σ) is 4 minutes in short cadence mode. TTV scales as orbital period P, and transit probability as $P^{-2/3}$, so that TTV $\sim$ (transit probability)$^{-3/2}$.

In addition to the orbital period P (the interval between transits) it may be possible to limit the orbital eccentricity of such transiting planets (Ford et al. 2008). To the extent that limb darkening effects can be accounted for, the orbital eccentricity can be constrained independently of the transit impact parameter by measuring the duration of both the transit T and the ingress and egress phases τ. The following relation holds:

$$\frac{1-e^2}{(1+e\sin\omega)^2} = \left(\frac{T\tau}{\sqrt{\delta}}\right)\left(\frac{\pi^2 G\rho_*}{3P}\right)^{2/3}, \quad (12)$$

where ρ_* is the density of the star, and ω is the argument of the periapsis (Seager & Mallén-Ornelas 2003; Tingley & Sackett 2005). To the first order in eccentricity, the term on the left is $1-2e\sin\omega$ and therefore only a minimum eccentricity can be established independently of the longitude of periapsis. However, the distribution of ω in a population of transiting systems must be uniform over $0-2\pi$ and thus the statistical distribution of e can be inferred. ρ_* is well established from astrophysical theory but will not be measured directly except in those cases where there is a second transiting planet either on a shorter period orbit that is accessible to the Doppler technique (Sozzetti et al. 2007) or via their mutual transit timing perturbations (Holman & Murray 2005).

The presence of an additional, outer planet of mass M_2 on an orbit with semimajor axis a_2 can be inferred through variations in the interval between transits (Miralda-Escudé 2002; Agol et al. 2005; Holman & Murray 2005). The standard deviation of the transit time due to perturbations from the outer planet is approximately

$$\delta T_c \approx \frac{P_1}{2^{3/2}\pi}\frac{a_2}{a_1}\frac{M_2}{M_*} \quad (13)$$

for nearly circular orbits (Agol et al. 2005). This will be typically $3\times10^{-6}P_1$, or ~ 5 min. If the second planet is near a mean-motion commensurability, the variation can be 1-3 orders of magnitude larger. We calculated the δT_c of the inner planet induced by the other planets in each of the 180 systems. These calculations used the orbited elements computed by Mercury for 100 successive orbits at 5 Gyr. The linear perturbations of the orbital equations are:

$$\delta T_c = \delta t_0 + \frac{P}{2\pi}\delta\mu + \frac{\mu}{2\pi}\delta P, \quad (14)$$

where

$$\delta\mu = (1-e\cos\eta)\delta\eta - (\sin\eta)\,\delta e, \quad (15)$$

and

$$\delta\eta = -\frac{\cos\omega\,(1-e\cos\eta)^2\,\delta\omega}{(1+e)\sin\eta - e\sin\eta\cos\eta} + \frac{[1-(1+e)\cos\eta]\,\delta e}{(1+e)\sin\eta - e\sin\eta\cos\eta}, \quad (16)$$

where t_0 is the time of periapsis passage, μ is the mean anomaly, and η is the eccentric anomaly. Figure 16 plots the δT_c versus transit probability for the innermost planets in the 180 simulation sets. Table 4 has the $\overline{\delta T_c}$ and transit probability values for each simulation set. Detection of TTV with *Kepler* obviously requires a third transit, and thus an extended mission, as well as read-out in short-cadence (59 s) mode to capture the ingress or egress (about 20 min in duration). The S/N of the transit detection over the ingress and egress is about 5, and the 1σ precision of the timing (using both ingress and egress) is about 3 min. Thus additional observations of transits by the innermost planet by *Kepler* should be sufficient to reveal the presence of outer planets like those predicted by our simulations. Observations from the ground have achieved ~ 0.5 mmag precision (Johnson et al. 2009; Southworth et al. 2009), raising the possibility that ground-based follow-up might also reveal such variation.

4.3. *Space Interferometry Mission (SIM-Lite)*

SIM-Lite is an astrometric interferometer mission that will achieve sub-microarcsecond precision per "visit" and should be capable of detecting Earth-mass planets in the habitable zone of nearby ($d < 30$ pc) stars (Shao & Nemati 2009). During a nominal program that consumes 40% of a 5 yr mission lifetime, 64 target stars can each be visited about 200 times. The total S/N in N visits is

$$S/N = F \times \frac{\sqrt{N}}{\sigma}\frac{a}{D}\frac{m_p}{M_*}, \quad (17)$$

where m_p is the mass of the planet, σ is the measurement error in arc-seconds, D is the distance in pc, and the dimensionless factor F is

$$F = \sqrt{\frac{1}{2}\left(1+\cos^2 i\right)\left[1-e^2\left[3-\left(\frac{2}{1+\cos^2 i}-1\right)\cos 2\omega\right]\right]} \quad (18)$$

(K. Mogren & B. S. Gaudi, i preparation, J. Catanzarite, private communication). Although planets with orbital periods longer than the mission lifetime might be detectable, we conservatively assume that this is not the case. Equation (18) is averaged over an isotropic distribution of values for i and ω, and the S/N is calculated for the 64 target stars for SIM-lite provided by J. Catanzarite. We adopt a detection criteria of S/N > 5.8 for a single planet (Catanzarite et al. 2006). We find that 96% of the innermost planets will be detected. If we assume $\sim$ 60% of stars have systems like those in our simulations and ignore planets with periods greater than the lifetime of the mission, we predict that SIM-lite will find 44 planets like those in our simulations (see Table 4). The presence of multiple planets may make disambiguation of orbital parameters difficult, but detection of additional planets in these systems is clearly possible. See Ford (2006) and Gould (2008) for more robust analyses of this problem.

5. DISCUSSION

5.1. *Summary*

Our simulations predict the evolution, final configuration and detection of systems of icy planets lacking gas giants. If, as observations indicate, all solar-mass stars are born with disks, but only a minority ($\sim$40%) form giant planets, our predictions may describe the hitherto "invisible" majority of outer planetary systems.

Because planet formation is so poorly understood, and there are few constraints on our simulations, we explore a wide range of initial conditions. We assume the canonical theory of planet formation in which a small number of oligarchs grow from a disk of much smaller planetesimals. Motivated by the core accretion theory of giant planet formation, we also assume that oligarchic growth was accelerated in a region of enhanced surface density of solids beyond the ice line, a hypothetical point in the planet-forming disk where water ice condenses. We do not simulate the formation of these oligarchs, only their subsequent growth and dynamics after the gas has disappeared from the disk. We assume that the longer orbital periods and lower surface density has stymied oligarch formation further out in the disk. The residual disk is represented by a finite number (typically 500) of small bodies. For increased computational efficiency, we place mass interior to the ice line in only a few realizations to investigate its effect.

We vary the total mass in the ice line, the location of the ice line, the initial number of oligarchs, and their spacing. We evolve each system for 5 Gyr; after the first Gyr the small bodies are removed. These systems are highly chaotic in the first 10 Myr, but usually become stable well before 1 Gyr, and removal of small bodies has no significant effect on the oligarchs' subsequent evolution. We describe the evolution of these systems in terms of the time to clear the oligarch zone of small bodies, the number of MMR crossings, the number of oligarch "swaps", the migration of the innermost oligarch, and the frequency of oligarch ejection (Table 2). We describe the final configuration of the systems at 5 Gyr using three statistics: the OSS, RMC, and AMD (Table 3). In a limited set of observations, we place mass interior to the ice line, either pairs of Earth Venus analogs, or smaller oligarchs, and we investigate its effect on the evolution of the outer system, as well as its own fate.

5.2. *Major conclusions and implications*

In the vast majority (169/180) of our primary runs, and *across all initial conditions we investigate*, an oligarch migrates interior to the ice line, settling to between 25% and 60% of the ice line distance in about 10 Myr and growing into a planet with a median mass of 0.23 $M_{\rm ice}$. We call this object the *innermost migrated planet*, or IMP. In 123 of the 169 primary runs with an IMP, the IMP is the most massive planet. IMPs are clearly distinguishable from the other planets (Figures 7 and 8). The migration is a result of exchange of angular momentum between the IMP and the other, exterior oligarchs: 5 of the 11 runs that did not produce an IMP contain only a single planet at 5 Gyr. The migration is significant because, unlike with gas giants, the planets in our simulations have low masses compared to the residual disk mass. The existence of mass in the inner system only slightly affects the final position and mass of IMP, but the converse is not true (see below). IMPs may be the visible representatives of an otherwise "invisible" majority: The common occurrence, relatively high mass, and small semimajor axis of IMPs make them eminently detectable by microlensing, transits (with *Kepler*), and astrometry (with SIM-Lite), but not yet by current Doppler capabilities.

Ground-based microlensing is currently capable of detecting planets as small as $\sim 3\ M_\oplus$ at separations of 1.5-3 AU, and indeed several planets with (uncertain) masses between a few $M_\oplus$ and one or two Neptunes have been found in this distance range (Beaulieu et al. 2006; Gould et al. 2006; Bennett et al. 2008; Sumi et al. 2010). These few detections may represent only the tip of the IMP-berg: all available constraints on the frequency of gas-giant and lower-mass planets from current radial velocity and microlensing surveys are consistent with the scenario that the minority of stars host gas giants, and that at least $\sim 60\%$ of stars host systems such as those we have simulated (Gould et al. 2006; Sumi et al. 2010). Future microlensing surveys will provide a definitive statistical measurement or upper limit on the frequency of systems like those predicted here. If 60% of stars indeed host systems similar to those we simulate, we estimate that next-generation ground-based microlensing surveys (Gould et al. 2007; Gould 2008; Gaudi et al. 2009) will detect $\sim$ 26 planets per year, including a handful of multiple-planet systems. A space-based microlensing survey would be sensitive to essentially all of the planets we have simulated (Bennett & Rhie 2002; Bennett et al. 2009; Beaulieu et al. 2010).

Assuming an ice-rock composition, all IMPs predicted here would produce a transit sufficiently deep to be detected by *Kepler*. 83% have periods less than the spacecraft's 3.5 yr mission. If IMPs are present around 60% of solar-type stars, we predict that *Kepler* will detect $\sim$129 of them with two or more transits. Observations of additional transits in high cadence (1 min resolution) mode in an extended *Kepler* mission could reveal additional, exterior planets through the variation of the timing of transits. Direct calculations show variations of 20-90 min in our predicted systems. Finally, SIM-Lite should be able detect 96% of IMPs.

The planets we predict have, statistically, very different orbital, mass, and eccentricity distributions than the giant planets discovered to date by Doppler surveys. The orbital eccentricities of our predicted planets are significantly lower than in known exoplanetary systems. Our results agree qualitatively with the simulations of systems of Neptune-size planets by Raymond et al. (2010). The exceptions are, unsurprisingly, our sets of simulations with dynamically overpacked oligarchs, whose orbital eccentricities at 5 Gyr resemble the observed exoplanet distribution. *Kepler* observations of the duration of transit ingress and/or egress will offer limited constraints on the distribution of eccentricities of IMPs, if they are sufficiently numerous.

If many more IMPs are found than predicted here, and they are closer to their parent star, then a possible explanation suggested by our simulations is that the ice line is often much closer than 5 AU from the parent star. Conversely, if the combination of microlensing, *Kepler*, and SIM-Lite fail to discover a population of IMPs, one or more assumptions in our scenario is false. The most likely suspect would be the assumption of a significant concentration of solids at or immediately beyond the ice line. This would have ramifications for the core accretion theory of giant planet formation.

Intriguingly, inner systems of two dominant planets are not stable in our scenario. In all simulations with Earth and Venus analogs, the two bodies collided, forming a single body at $\sim$ 0.8 AU. No contradiction with

the solar system is engendered because it contains giant planets. Such a conglomerate would induce a barycenter motion of 0.2 m s^{-1} (260 d period) which may be detectable by future ultra-high precision Doppler monitoring (Pepe & Lovis 2008). On the other hand, if planet formation in the inner system has progressed only to the giant impact (oligarch-dominated) phase by the time the IMP migrates inward, the IMP will clear most of this mass, leaving only small ($< 0.3\ M_\oplus$) bodies.

If disruption of the inner system does occur, the IMP is left as the only detectable planet near, but exterior to, the nominal habitable zone of an Earth "twin" (0.95-1.37 AU) (Kasting et al. 1993). However, it is expected that surface temperatures will be higher on more massive planets with thicker atmospheres, such as could be the case for the IMP. Given that IMPs have large quantities of water, it then follows that IMP-like planets could be the most numerous type of habitable planet in the universe.

5.3. *Limitations of our simulations*

We have ignored Type I migration in our simulation. However, the magnitude and even the sign of Type I migration is not yet clear (Li et al. 2009; Muto & Inutsuka 2009; Ogihara & Ida 2009; Yu et al. 2010). Our results are best seen in the context of being an end-member of a larger suite of scenarios in which Type I migration plays a role to a varying degree, c.f. Ida & Lin (2008a).

Planetesimals will fragment (rather than accrete) if the collisional energy exceeds the strength of the colliders, and the production of smaller fragments can eventually produce a collisional "cascade" whose ultimate product is micron-sized dust which will be swept from the disk by radiation forces or coupling to the gas disk (Wyatt 2008). After the gas disk disappears, the orbital eccentricities and inclinations of planetesimals are no long damped, and they will be excited by the oligarchs, which are growing by accretion of planetesimals. Thus fragmentation will compete with oligarch accretion and may limit oligarch growth to some maximum mass. In a collisional cascade, most of the mass will be in the largest planetesimals and thus it is their lifetime that will set the balance between accretion and fragmentation. The strength of these will be set by gravity and will depend on on size as $s^{3/2}$ (Krivov et al. 2005), and thus the critical collision speed for fragmentation will scale as $s^{3/4}$, e.g., 1 km s^{-1} for a 100 km body (Löhne et al. 2008). The equilibrium velocities of the planetesimals will scale with those of the oligarchs by the ratio of mass surface densities in the respective populations $\left(\frac{\Sigma_l}{\Sigma_s}\right)^n$ where $n \approx 0.25 - 0.5$ (e.g., Goldreich et al. (2004)). Thus as planetesimals are accreted and oligarchs grow, the collision speeds of the former will increase until the largest planetesimals suffer destructive collisions, after which that process competes effectively with accretion for mass. Unfortunately, neither the size of the largest planetesimals (which may ultimately derive from physics such as two-stream instabilities (Johansen et al. 2007). However, once $\Sigma_l \sim \Sigma_p$, v_p will become comparable to the escape speed of the oligarchs ($\sim$ 10 km s^{-1}) and probably well above the threshold for fragmentation. Thus a crude upper limit on the effect of fragmentation is the mass of the oligarchs when the surface density of planetesimals fall below the surface density of oligarchs. In the standard set of simulations, this is usually after $\sim$ 100 Myr. Direct evaluation of the RMS encounter velocity of planetesimals in our standard sets show that this kinetic energy increases with time until it reaches 10% of the orbital kinetic energy (i.e., $v \sim 4$ km s^{-1}) in $\sim$ 100 Myr. Oligarchs have accreted $\sim$ 80% of their mass by this time. Orbital migration, which depends on the mass surface density of the planetesimals, and not their mass distribution, will be affected less.

Our scenario assumes a significant concentration of mass within 1 AU of the ice line, with a total amount sufficient to produce least one and as many as four of the supposed 5-10 $M_\oplus$ cores of the outer planets in our solar system. If the total mass in the ice line was less, or it was less concentrated then we assume, the result would be smaller bodies, and the amount of inward migration by the innermost object would be less.

Our systems are all orbiting solar-mass stars, whereas those surveyed by *Kepler* comprise a range of stellar masses (Batalha et al. 2010), and the preponderance of microlensing stars are lower mass M dwarfs ($< 0.5 M_\odot$). Observations suggest a correlation between stellar mass and giant planet frequency, at least on detectable orbits (Johnson et al. 2007), and in line with some theoretical expectations (Kennedy & Kenyon 2008b). At a given ice line distance, the orbital time scale is longer and the Safronov number scales inversely with stellar mass. We thus expect those systems around M dwarfs to develop more slowly and scattering to be more efficient relative to accretion. A prediction of the latter is a higher mean orbital eccentricity among the planets than the values found here. However, a correlation between disk mass and stellar mass, if one exists (Natta et al. 2000; Eisner et al. 2008; Vorobyov 2009), along with our finding that the mass of the IMP approximately scales with the mass in the ice line, would partially offset this effect. Moreover, the ice line itself may be closer to the star (Kennedy & Kenyon 2008b), and thus both the orbital time scale and Safronov number will depend only weakly on stellar mass.

Given these unresolved issues, our findings should be considered a series of predictions of one class of planets that could be (and perhaps is being) discovered by microlensing, *Kepler*, and a future SIM-Lite mission. If gas giant-containing systems are indeed in the minority, then systems of icy Earth-to-Neptune-mass planets may be the hitherto undiscovered majority of planet systems, and their innermost members - the IMPs - could be one of the most common abodes for life in the universe. Assuming the continued success of microlensing surveys and planet-finding missions like *Kepler*, we shall soon know the answer.

This research was supported in part by the National Science Foundation through TeraGrid (Catlett et al. 2007) resources provided by Purdue University. Sean Raymond provided code to search for MMR. AM and EG are supported by NSF grant AST0908419. We thank Joe Catanzarite for assistance with the SIM-Lite detection calculations and providing a nominal target list, Andy Gould and Cheongho Han for permission to use unpublished simulations, and Karen Mogren for permission to include results from work in preparation. We thank an

anonymous reviewer for helpful comments and suggestions.

REFERENCES

Abe, Y., Ohtani, E., Okuchi, T., Righter, K., & Drake, M. 2000, Water in the Early Earth, ed. Canup, R. M., et al., 413–433
Adams, F. C., & Laughlin, G. 2003, Icarus, 163, 290
Agol, E., Steffen, J., Sari, R., & Clarkson, W. 2005, MNRAS, 359, 567
Andrews, S. M., & Williams, J. P. 2007, ApJ, 659, 705
Asplund, M., Grevesse, N., Sauval, A. J., & Scott, P. 2009, ARA&A, 47, 481
Ayliffe, B. A., & Bate, M. R. 2009, MNRAS, 393, 49
Batalha, N. M., et al. 2010, ApJ, 713, L109
Beaulieu, J., et al. 2006, Nature, 439, 437
Beaulieu, J. P., et al. 2010, ArXiv e-prints
Bennett, D. P., & Rhie, S. H. 2002, ApJ, 574, 985
Bennett, D. P., et al. 2008, ApJ, 684, 663
Bennett, D. P., et al. 2009, in Astronomy, Vol. 2010, astro2010: The Astronomy and Astrophysics Decadal Survey, 18–+
Carpenter, J. M., et al. 2009, ApJS, 181, 197
Catanzarite, J., Shao, M., Tanner, A., Unwin, S., & Yu, J. 2006, PASP, 118, 1319
Catlett, C., et al. 2007, Advances in Parallel Computing, 9
Chambers, J. 2006, Icarus, 180, 496
Chambers, J. E. 1999, MNRAS, 304, 793
—. 2001, Icarus, 152, 205
Chatterjee, S., Ford, E. B., Matsumura, S., & Rasio, F. A. 2008, ApJ, 686, 580
Ciesla, F. J., & Cuzzi, J. N. 2006, Icarus, 181, 178
Collins, B. F., & Sari, R. 2009, AJ, 137, 3778
Crida, A., Masset, F., & Morbidelli, A. 2009, ApJ, 705, L148
Cumming, A. 2004, MNRAS, 354, 1165
Cumming, A., Butler, R. P., Marcy, G. W., Vogt, S. S., Wright, J. T., & Fischer, D. A. 2008, PASP, 120, 531
Currie, T. 2009, ApJ, 694, L171
Cuzzi, J. N., & Zahnle, K. J. 2004, ApJ, 614, 490
D'Antona, F., & Mazzitelli, I. 1994, ApJS, 90, 467
Debes, J. H., & Sigurdsson, S. 2006, A&A, 451, 351
—. 2007, ApJ, 668, L167
Di Stefano, R., & Scalzo, R. A. 1999a, ApJ, 512, 564
—. 1999b, ApJ, 512, 579
Eggenberger, A., & Udry, S. 2010, in EAS Publications Series, Vol. 41, EAS Publications Series, ed. T. Montmerle, D. Ehrenreich, & A.-M. Lagrange, 27–75
Eisner, J. A., Plambeck, R. L., Carpenter, J. M., Corder, S. A., Qi, C., & Wilner, D. 2008, ApJ, 683, 304
Elliot, J. L., et al. 2005, AJ, 129, 1117
Evans, N. J., et al. 2009, ApJS, 181, 321
Fischer, D. A., & Valenti, J. 2005, ApJ, 622, 1102
Ford, E. B. 2006, PASP, 118, 364
Ford, E. B., & Chiang, E. I. 2007, ApJ, 661, 602
Ford, E. B., Quinn, S. N., & Veras, D. 2008, ApJ, 678, 1407
Ford, E. B., Rasio, F. A., & Sills, A. 1999, ApJ, 514, 411
Gaudi, B. S., et al. 2009, in Astronomy, Vol. 2010, astro2010: The Astronomy and Astrophysics Decadal Survey, 85–+
Gladman, B. 1993, Icarus, 106, 247
Goldreich, P., Lithwick, Y., & Sari, R. 2004, ApJ, 614, 497
Gomes, R., Levison, H. F., Tsiganis, K., & Morbidelli, A. 2005, Nature, 435, 466
Gonzalez, G. 1999, MNRAS, 308, 447
—. 2006, PASP, 118, 1494
Gould, A. 2008, arXiv:0807.4323
Gould, A., Gaudi, B. S., & Bennett, D. P. 2007, ArXiv e-prints
Gould, A., et al. 2006, ApJ, 644, L37
—. 2010, ArXiv e-prints
Grasset, O., Schneider, J., & Sotin, C. 2009, ApJ, 693, 722
Grevesse, N., & Anders, E. 1989, in American Institute of Physics Conference Series, Vol. 183, Cosmic Abundances of Matter, ed. C. J. Waddington, 1–8
Hahn, J. M., & Malhotra, R. 1999, AJ, 117, 3041
Haisch, Jr., K. E., Lada, E. A., & Lada, C. J. 2001, ApJ, 553, L153
Han, C., Gaudi, B. S., An, J. H., & Gould, A. 2005, ApJ, 618, 962
Han, C., & Gould, A. 1995, ApJ, 447, 53
—. 2003, ApJ, 592, 172
Holman, M. J., & Murray, N. W. 2005, Science, 307, 1288
Hubbard, W. B., Dougherty, M. K., Gautier, D., & Jacobson, R. 2009, The Interior of Saturn, ed. Dougherty, M. K., Esposito, L. W., & Krimigis, S. M., 75–81
Hubickyj, O., Bodenheimer, P., & Lissauer, J. J. 2005, Icarus, 179, 415
Ida, S., Bryden, G., Lin, D. N. C., & Tanaka, H. 2000, ApJ, 534, 428
Ida, S., & Lin, D. N. C. 2004a, ApJ, 604, 388
—. 2004b, ApJ, 616, 567
—. 2008a, ApJ, 673, 487
—. 2008b, ApJ, 685, 584
Jenkins, J. M., et al. 2010, ApJ, 713, L120
Johansen, A., Oishi, J. S., Low, M., Klahr, H., Henning, T., & Youdin, A. 2007, Nature, 448, 1022
Johnson, J. A., Butler, R. P., Marcy, G. W., Fischer, D. A., Vogt, S. S., Wright, J. T., & Peek, K. M. G. 2007, ApJ, 670, 833
Johnson, J. A., Winn, J. N., Cabrera, N. E., & Carter, J. A. 2009, ApJ, 692, L100
Jurić, M., & Tremaine, S. 2008, ApJ, 686, 603
Kalas, P., et al. 2008, Science, 322, 1345
Kasting, J. F., Whitmire, D. P., & Reynolds, R. T. 1993, Icarus, 101, 108
Kennedy, G. M., & Kenyon, S. J. 2008a, ApJ, 682, 1264
—. 2008b, ApJ, 673, 502
Kenyon, S. J., & Bromley, B. C. 2006, AJ, 131, 1837
—. 2009, ApJ, 690, L140
—. 2010, ApJS, 188, 242
Koch, D. G., et al. 2010, ApJ, 713, L79
Kokubo, E., & Ida, S. 2002, ApJ, 581, 666
Kornet, K., Różyczka, M., & Stepinski, T. F. 2004, A&A, 417, 151
Krivov, A. V., Sremčević, M., & Spahn, F. 2005, Icarus, 174, 105
Lada, C. J., et al. 2006, AJ, 131, 1574
Laughlin, G., Bodenheimer, P., & Adams, F. C. 2004, ApJ, 612, L73
Li, H., Lubow, S. H., Li, S., & Lin, D. N. C. 2009, ApJ, 690, L52
Lineweaver, C. H., & Grether, D. 2003, ApJ, 598, 1350
Lissauer, J. J. 1987, Icarus, 69, 249
Lodders, K. 2003, ApJ, 591, 1220
Löhne, T., Krivov, A. V., & Rodmann, J. 2008, ApJ, 673, 1123
Luhman, K. L., Allen, P. R., Espaillat, C., Hartmann, L., & Calvet, N. 2010, ApJS, 186, 111
Luhman, K. L., et al. 2008, ApJ, 675, 1375
Malhotra, R. 1993, Nature, 365, 819
Marois, C., Macintosh, B., Barman, T., Zuckerman, B., Song, I., Patience, J., Lafrenière, D., & Doyon, R. 2008, Science, 322, 1348
Massi, F., di Carlo, E., Codella, C., Testi, L., Vanzi, L., & Gomes, J. I. 2010, A&A, 516, A52+
Miralda-Escudé, J. 2002, ApJ, 564, 1019
Mordasini, C., Alibert, Y., Benz, W., & Naef, D. 2009, A&A, 501, 1161
Muto, T., & Inutsuka, S. 2009, ApJ, 701, 18
Natta, A., Grinin, V., & Mannings, V. 2000, Protostars and Planets IV, 559
Nelson, A. F., & Angel, J. R. P. 1998, ApJ, 500, 940
Ogihara, M., & Ida, S. 2009, ApJ, 699, 824
Pätzold, M., & Rauer, H. 2002, ApJ, 568, L117
Pepe, F. A., & Lovis, C. 2008, Physica Scripta Volume T, 130, 014007
Pinsonneault, M. H., DePoy, D. L., & Coffee, M. 2001, ApJ, 556, L59
Pollack, J. B., Hubickyj, O., Bodenheimer, P., Lissauer, J. J., Podolak, M., & Greenzweig, Y. 1996, Icarus, 124, 62
Pringle, J. E. 1981, ARA&A, 19, 137
Quillen, A. C. 2002, AJ, 124, 400
Rafikov, R. R. 2004, AJ, 128, 1348
Rasio, F. A., & Ford, E. B. 1996, Science, 274, 954
Raymond, S. N., Armitage, P. J., & Gorelick, N. 2009a, ApJ, 699, L88
—. 2010, ApJ, 711, 772
Raymond, S. N., Barnes, R., Armitage, P. J., & Gorelick, N. 2008, ApJ, 687, L107

Raymond, S. N., Barnes, R., Veras, D., Armitage, P. J., Gorelick, N., & Greenberg, R. 2009b, ApJ, 696, L98
Raymond, S. N., O'Brien, D. P., Morbidelli, A., & Kaib, N. A. 2009c, Icarus, 203, 644
Scharf, C., & Menou, K. 2009, ApJ, 693, L113
Seager, S., & Mallén-Ornelas, G. 2003, ApJ, 585, 1038
Selsis, F., et al. 2007, Icarus, 191, 453
Shao, M., & Nemati, B. 2009, PASP, 121, 41
Sicilia-Aguilar, A., et al. 2006, ApJ, 638, 897
Southworth, J., et al. 2009, MNRAS, 399, 287
Sozzetti, A., Torres, G., Charbonneau, D., Latham, D. W., Holman, M. J., Winn, J. N., Laird, J. B., & O'Donovan, F. T. 2007, ApJ, 664, 1190
Stevenson, D. J. 1999, Nature, 400, 32
Stevenson, D. J., & Lunine, J. I. 1988, Icarus, 75, 146
Sumi, T., et al. 2010, ApJ, 710, 1641
Thalmann, C., et al. 2009, ApJ, 707, L123
Thommes, E. W., Duncan, M. J., & Levison, H. F. 2002, AJ, 123, 2862
Thommes, E. W., Matsumura, S., & Rasio, F. A. 2008, Science, 321, 814
Tingley, B., & Sackett, P. D. 2005, ApJ, 627, 1011
Udry, S., Mayor, M., & Santos, N. C. 2003, A&A, 407, 369
Udry, S., & Santos, N. C. 2007, ARA&A, 45, 397
Veras, D., Crepp, J. R., & Ford, E. B. 2009, ApJ, 696, 1600
Vorobyov, E. I. 2009, ApJ, 692, 1609
Wyatt, M. C. 2008, ARA&A, 46, 339
Yee, J. C., & Gaudi, B. S. 2008, ApJ, 688, 616
Yu, C., Li, H., Li, S., Lubow, S. H., & Lin, D. N. C. 2010, ApJ, 712, 198